UNIVERSITY OF CALIFORNIA SAN DIEGO

High-Resolution Observations of South Pacific Low Latitude Western Boundary Currents

A Thesis submitted in partial satisfaction of the requirements
for the degree Master of Science

in

Oceanography

by

Scarlett Hensman

Committee in charge:

Nathalie Zilberman, Chair
Mark Merrifield
Janet Sprintall

2023

The Thesis of Scarlett Hensman is approved, and it is acceptable in quality and form for publication on microfilm and electronically.

University of California San Diego

2023

TABLE OF CONTENTS

LIST OF FIGURES

LIST OF TABLES

LIST OF ABBREVIATIONS

AAIW	Antarctic Intermediate Water
CT	Conservative Temperature
EAC	East Australian Current
ENSO	El Niño Southern Oscillation
EUC	Equatorial Undercurrent
GPC	Gulf of Papua Current
HR-XBT	High-Resolution Expendable Bathythermograph
ITF	Indonesian Throughflow
LLWBCs	Low Latitude Western Boundary Currents
LTW	Lower Thermocline Waters
NBCU	New Britain Coastal Undercurrent
NCJ	North Caledonian Jet
NECC	North Equatorial Countercurrent
NGCC	New Guinea Coastal Current
NGCU	New Guinea Coastal Undercurrent
NICU	New Ireland Coastal Undercurrent
NQC	North Queensland Current
NVJ	North Vanuatu Jet
SA	Absolute Salinity
SAMW	Subantarctic Mode Water
SEC	South Equatorial Current
SGU	St. George Undercurrent
SICU	Solomon Island Coastal Undercurrent
SLA	Sea Level Anomaly
SLAs	Sea Level Anomalies
SLW	Subtropical Lower Water
SPSTW	South Pacific Subtropical Water
SPTW	South Pacific Tropical Water
STMW	Subtropical Mode Water
TS	Temperature-Salinity
UTW	Upper Thermocline Waters

ACKNOWLEDGEMENTS

High Resolution Expendable Bathythermograph (HR-XBT) data is made available by the Scripps Institution of Oceanography High Resolution XBT/XCTD Program (http://www-hrx.ucsd.edu/). Argo data was collected and made freely available by the International Argo Program and the national programs that contribute to it (http://www.argo.ucsd.edu, http://argo.jcommops.org). The Argo Program is part of the Global Ocean Observing System. High-resolution Argo climatology is available at http://sio-argo.ucsd.edu/RG_Climatology.html. Satellite altimetry is made available by Copernicus Marine Service (https://marine.copernicus.eu/).

The thesis author was the primary investigator and author of this paper. While the discovery of the shallow, fast, and persistent flow in the central Solomon Sea appears new to oceanographic literature, it may be familiar to Indigenous peoples. Therefore if future investigations confirm this flow as part of a surface current, they are implored to consider the knowledge of Indigenous peoples as much as oceanographic literature.

ABSTRACT OF THE THESIS

High-Resolution Observations of South Pacific Low Latitude Western Boundary Currents

by

Scarlett Hensman

Master of Science in Oceanography

University of California San Diego, 2023

Nathalie Zilberman, Chair

South Pacific Low Latitude Western Boundary Currents (LLWBCs) establish the major connection between the South Pacific subtropical gyre and the Equatorial Pacific. Despite their immense potential in influencing global thermohaline circulation and modulating the El Niño Southern Oscillation, South Pacific LLWBCs are largely undocumented through observations. This study provides a high-resolution investigation of the pathways and properties of the

Solomon Sea's LLWBCs using high-resolution expendable bathythermographs (HR-XBTs), Argo hydrographic surveys, and satellite altimetry. Combined Argo+HR-XBT data was used to calculate near 16-year time-mean conservative temperature, absolute salinity, potential density, dynamic height, and geostrophic velocity. Combined Argo+HR-XBT+Altimetry data was used to investigate monthly and seasonal conservative temperature, absolute salinity, and geostrophic velocity. Key findings include: (1) identification of five water masses within the Solomon Sea; (2) a shallow freshwater pool in the central Solomon Sea moving northward in austral spring; (3) southern/northern cores (~425m and ~250m depth respectively) of the Gulf of Papua Current reaching the surface when strengthened; (4) southern/northern cores of the New Guinea Coastal Undercurrent and New Guinea Coastal Current flowing at speeds 0.26m/s (~230m depth) and 0.2m/s (0-270m depth) respectively; (5) the discovery of a shallow, fast, and persistent (~0.42m/s) eastward flow in the central Solomon Sea; (6) flow speeds near 0.38m/s for the Solomon Strait inflow; (7) the New Britain Coastal Undercurrent (~0.24m/s between 260-450m depth) connects to an eastward surface flow from June-November; (8) a highly variable and indistinct New Ireland Coastal Undercurrent; (9) improved understanding of the flow reversals and subsurface flows from ~3°S-1°S.

1. INTRODUCTION

1.1 South Pacific Low Latitude Western Boundary Currents

Low latitude western boundary currents (LLWBCs) are essential features of the global climate system. As the major pathway between the central South Pacific and Equatorial Pacific, South Pacific LLWBCs transport physical properties from the South Pacific subtropical gyre to the Equatorial Undercurrent (EUC), Indonesian throughflow (ITF), and the Western Pacific warm pool (Butt-Lindstrom, 1994; Lukas et al., 1996). The South Pacific LLWBCs in turn affect global thermohaline circulation, El Niño Southern Oscillation (ENSO), and atmospheric processes like convection and precipitation (Lukas et al., 1996).

The critical role played by LLWBCs in carrying subtropical waters to the equator is attained through shallow, wind and buoyancy-driven subtropical circulation cells. These cells experience equatorial upwelling, poleward Ekman transport of surface waters from the equator, subduction within the subtropical gyre, and a returning geostrophic flow in the thermocline (Lukas et al., 1996).

Scientists anticipate the impact of increased equatorial warming will be seen through heightened equatorial convection, intensified southeasterly trade winds, and reduced meridional sea surface temperature gradients in the South Pacific (Ganachaud et al., 2014). Changes in atmospheric processes may place new challenges on Pacific Islander's freshwater supplies by altering rainfall patterns (Ganachaud et al., 2014). Furthermore, modifications in the trade winds will impact hurricane pathways, as well as global climate through ENSO. The effects of weakened sea surface temperature gradients in the South Pacific are yet to be understood. As a major mechanism within equatorial heat, salt, and mass budgets, the South Pacific LLWBCs are worthy of further investigation.

Previous studies highlight the seasonal and interannual variability of South Pacific LLWBCs when considering their characteristics and their impact on equatorial budgets. The South Pacific LLWBCs experience seasonally alternating monsoon circulations with wind variability greater than other LLWBCs (Lukas et al., 1996). Moreover, Anutaliya et al. (2019) portray that equatorward flow through the Solomon Sea is strongly influenced by ENSO signals with strengthened equatorward flow during El Niño and weakened equatorward flow during La Niña. Ganachaud et al. (2014) similarly find that the transport entering the New Guinea Coastal Undercurrent (NGCU), a significant component within the South Pacific LLWBC system, enhances during El Niño, and that the equatorward transport is reduced during La Niña.

1.2 Circulation pathways in the Southwest Pacific

The South Pacific LLWBC system is convoluted due to the complex bathymetry of the islands and deep ocean canyons spanning the Coral and Solomon Seas. The South Pacific LLWBCs are fed by many streams of the South Equatorial Current (SEC) as they break off from the South Pacific subtropical gyre. The southernmost SEC stream travels between New Caledonia and the Vanuatu Archipelago into the Coral Sea, forming the North Caledonian Jet (NCJ). Similarly, the North Vanuatu Jet (NVJ) is formed when a section of the SEC passes between the Vanuatu Archipelago and the Solomon Islands into the Coral and Solomon Sea regions. Upon encountering the Solomon Islands, a portion of the SEC may form the Solomon Island Coastal Undercurrent (SICU) that flows along the northern coastline of the Solomon Islands. The SICU is an undercurrent predicted in models though not yet confirmed through observations (Melet et al., 2010). Finally, the SEC contributes to Solomon Sea inflow before contacting New Ireland and the New Ireland Coastal Undercurrent (NICU).

The NCJ bifurcates upon reaching Australia's eastern coast; part of the NCJ travels south into the East Australian Current (EAC) while another portion of the NCJ enters the Gulf of Papua. In the Gulf of Papua, the NCJ forms the Gulf of Papua Current (GPC). The GPC flows equatorward alongside the land masses of northern Australia and southern Papua New Guinea before pivoting at the Louisiade Archipelago and finally joining the Solomon Sea. Upon entering the Solomon Sea, the GPC becomes a narrow, bounded current enhanced with the NVJ to form the New Guinea Coastal Current (NGCC) and the NGCU. Although the NVJ directly feeds into the NGCC and NGCU, the NGCU is primarily fed by the GPC, which may additionally be sourced from both the North Queensland Current (NQC) and the NVJ (Melet et al., 2010). With the NGCU established, the primary component of the South Pacific LLWBC system is in place (Ganachaud et al., 2014; Anutaliya et al., 2019).

The NGCC and NGCU are powerful currents traveling up the western side of the Solomon Sea. Upon reaching the northern Solomon Sea, the NGCU breaks into two streams: one continuing through the Vitiaz Strait and the other traveling parallel to the island of New Britain, thus forming the New Britain Coastal Undercurrent (NBCU). The Vitiaz Strait is one of three major connections between the Solomon Sea and the equator; it spans 42 km wide and is 1000 m deep (Melet et al., 2010). The remaining major pathways between the Solomon Sea to the equator include St. George's Channel (a passage 15-km wide and 1,400 m deep) and the Solomon Strait (a passage 185 km wide and 2,525 m deep. Melet et al., 2010; Alberty et al., 2019). The NBCU leaves through both St. George's Channel and the Solomon Strait. The lesser portion of the NBCU forms the St. George Undercurrent (SGU) when entering St. George's Channel (Alberty et al., 2019). The SGU then deflects west within the Bismarck Sea to recombine with the NGCU along the northern portion of Papua New Guinea where it continues its path of strong, equatorward flow. Models

suggest that the greater portion of the NBCU exiting the Solomon Strait may cross paths with the SICU before becoming a major contributor to the NICU (Melet et al., 2010).

The modeling study of Melet et al. (2010) proposed the SICU is bounded to a 100-km width along the east side of the Solomon Islands with mean speeds of 20 cm/s at 200 m depth. In their review, Ganachaud et al. (2014) remark on the SICU's potential in being a source for the Solomon Sea Inflow (waters entering the Solomon Sea at thermocline depths through the Solomon Strait) and offer the contrasting model finds of Hristova et al. (2014) and Djath et al. (2014b) depicting flow of varying directions and strong seasonal variability east of the Solomon Islands.

The NICU was found traveling equatorward within 40 km of New Ireland's eastern coast by Butt-Lindstrom (1994). The model results of Melet et al. (2010) proposed the NICU is not only fed by the SEC at thermocline depths, but also the NBCU and SICU. At 2°S the NICU branches in two directions: a small portion of the NICU heads west to merge with the NGCU while the greater portion of the NICU follows a more direct path to the equator and flows uninterrupted into the EUC. This direct path of the NICU forms the major connection of the Solomon Sea and EUC at thermocline depths and fuels the North Equatorial Countercurrent (NECC; Melet et al., 2010). The NICU portion that connects with the NGCU flows eastward into the ITF. The ITF is the tropical path Pacific waters can take into the Indian Ocean (Lukas et al., 1996).

In contrast to the major currents to the west, the southern entrance and eastern portion of the Solomon Sea are characterized by weak mesoscale eddies and recirculation (Anutaliya et al. 2019; Melet et al. 2010). The Indispensable Strait (50 km wide and 1,400 m deep) is an additional pathway for waters at thermocline depth to enter the southern Solomon Sea (Alberty et al. 2019; Ganachaud et al. 2014).

1.3 Objectives

The complexity of the islands, ocean basins, and deep trenches spanning the Solomon Sea region has long stunted scientist's understanding of the South Pacific LLWBC system. A comprehensive image of the spatial and temporal features within the Solomon Sea region has been delayed by our inability to adequately survey the intricate region for periods long enough to resolve long-term variability. Here, we investigated the spatial (i.e., depth, width) and temporal (i.e., monthly, seasonal) variability of the circulation patterns governing the Solomon Sea and their properties using long-term observations from high-resolution expendable bathythermograph (HR-XBT) transects, sea surface height from satellite altimetry, and Argo hydrographic observations.

2. DATA AND METHODOLOGY

2.1 Data

The HR-XBT network collects temperature measurements from the surface to 800 m along near-repeat global shipping routes. This study focused on a segment (13°S-1°S) of the PX05 transect which transits from Brisbane, Australia through the Solomon Sea to Yokohama, Japan. Temperature profiles have been actively gathered along this path with two to four cruises per year during the years of 2009-2019 (Table 1 and Figure 1). Though a portion of the deeper transport is omitted from this source due to its 800 m depth limit, key characteristics of the South Pacific LLWBCs are anticipated to reside within the upper 800 m. HR-XBT data are available at https://www-hrx.ucsd.edu/.

Argo floats autonomously profile temperature and salinity within the upper 2000 m. Since 2007, the Argo program has achieved a 3˚ x 3˚ x 10-day global coverage capable of resolving seasonal and longer time scales across all oceans. As seen in Figure 2, Argo float distribution is sensitive to bathymetry. Between 2004 and 2019, 96% of Argo floats reached depths of 1000 m

within ±1° of the PX05 nominal transect, however only 86% reached 1200 m, 83% reached 1400 m, and 63% reached 1975 m. The bathymetry east of the Solomon Strait and New Ireland largely prevents floats from descending to 2000 m depth. There is also a cluster of floats unable to surpass 1000 m south of the Louisiade Archipelago despite being seemingly unburdened by bathymetry.

Table 1. PX05 cruises from 2009-2019.

Year	Jan	Feb	Mar	Apr	May	June	July	Aug	Sept	Oct	Nov	Dec	Total Cruises per Year
2009								908		910			2
2010	1001				1005			1008		1010			4
2011		1102			1105		1107			1110			4
2012			1203		1205			1208		1210			4
2013	1301				1305		1307			1310			4
2014					1405				1409		1411		3
2015		1502				1506			1509		1511		4
2016		1602			1605			1608		1610			4
2017	1701				1705			1708		1710			4
2018	1801			1804			1807			1810			4
2019	1901			1904			1907						3
Total Cruises per Month	5	3	1	2	7	1	4	5	2	8	2	0	

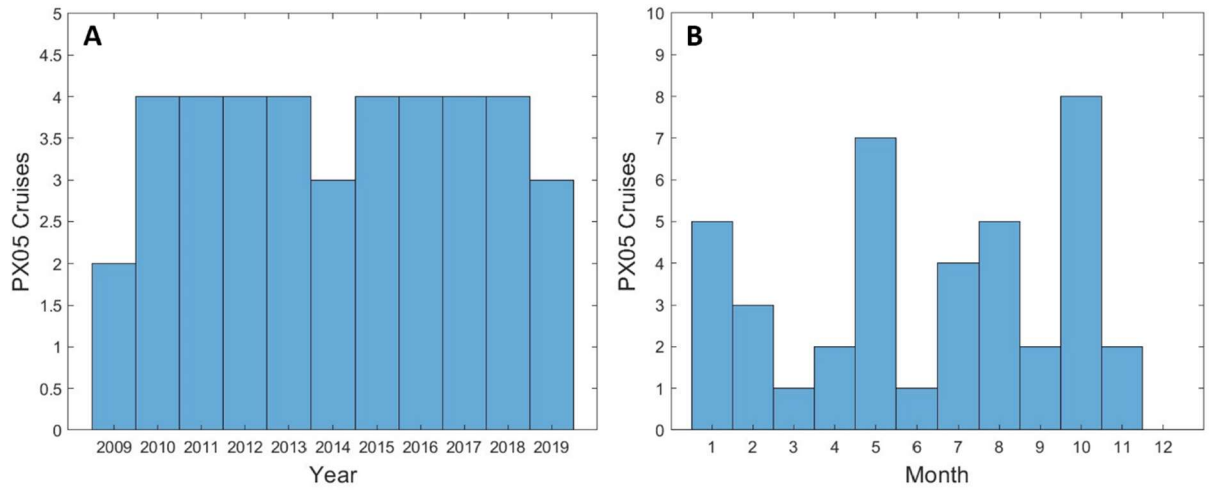

Figure 1. PX05 cruises per year (A) followed by PX05 cruises per month (B).

Satellite altimetry provides sea surface height through daily-mean sea level anomalies (SLAs) and monthly-mean SLAs. The satellite measurements used were the "Global Ocean

Gridded L4 Sea Surface Heights and Derived Variables Reprocessed (1993-ongoing)" dataset provided by the EU Copernicus Marine Service. Both the daily-mean and monthly-mean information were referenced to the 1993-2012 period and projected onto a 1/4°×1/4° grid. The daily-mean SLAs span 2004 to October 15th, 2019, while the monthly-mean SLAs span 2004 to September 2019. This dataset is suitable for investigating the time variability of geostrophic velocity and transport of LLWBCs (Zilberman et al., 2018; Chandler et al., 2021).

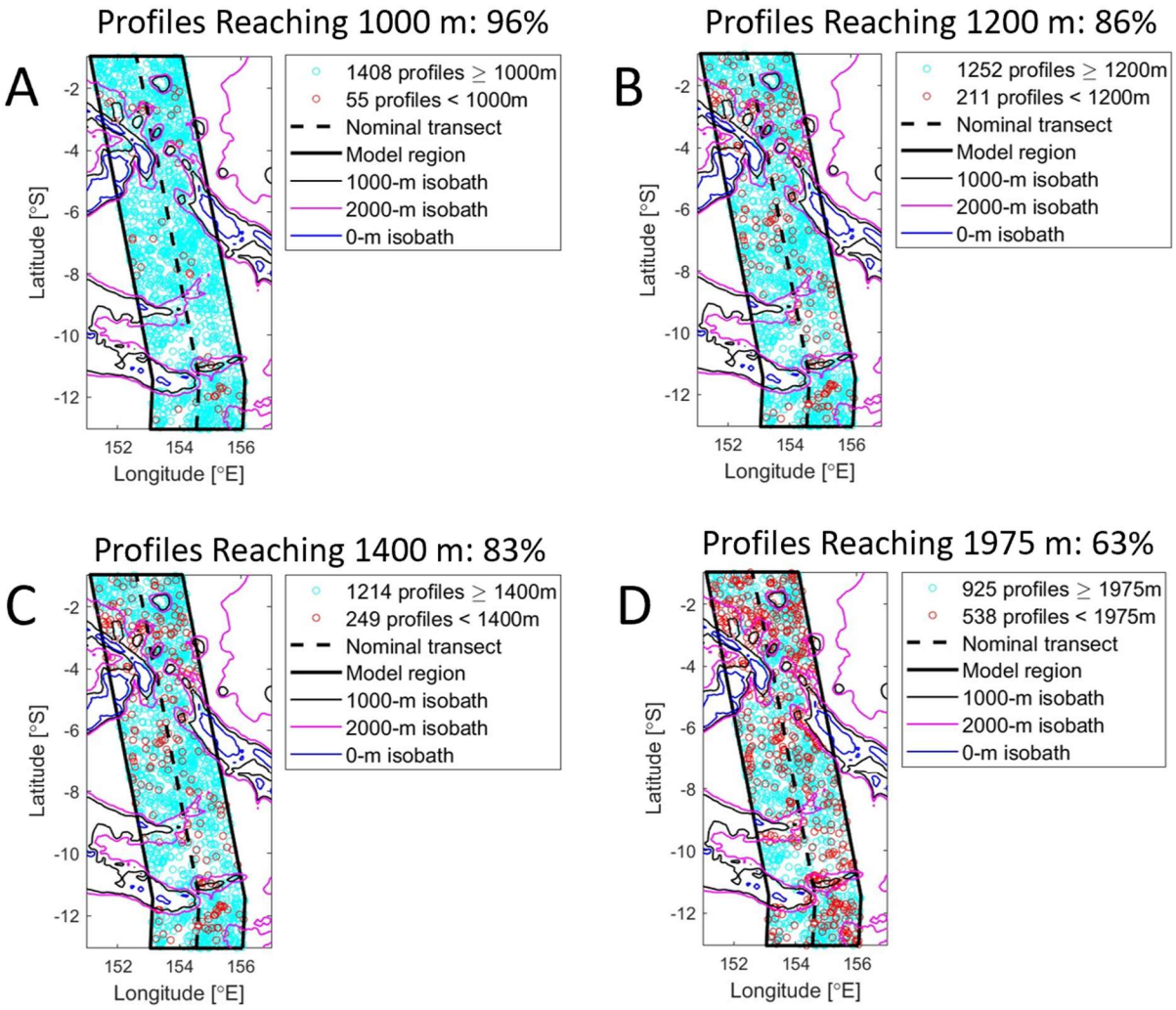

Figure 2. Individual Argo profiles reaching (A) at least 1000 m, (B) 1200 m, (C) 1400 m, and (D) 1975 m depth. Profiles are confined within ±1° of the PX05 HR-XBT nominal transect for the years 2004-2019.

2.2 Methodology

This study primarily relied on Argo climatology in conjunction with HR-XBTs (Argo+HR-XBT) for near 16-year time-mean ("general") investigations, and Argo climatology combined with HR-XBTs and satellite altimetry (Argo+HR-XBT+Altimetry) for monthly investigations within and surrounding the Solomon Sea over the same near 16-year period (2004-2019).

To first examine the characteristics of the South Pacific LLWBCs, dynamic height (0/1975 m) was calculated using Argo climatological data and interpolated around the Solomon Sea region. Roemmich and Gilson (2009) constructed a high-resolution (1/6°×1/6°) grid of mean Argo temperature and salinity climatologies through a weighted least squares fit using 58 standard pressure levels and 33 monthly profiles. Argo climatology relies on the 2004-2018 mean, which is not significantly different from the 2004-2019 mean (Chandler et al. 2021).

For the Argo+HR-XBT dataset, Argo and HR-XBT temperature measurements were objectively mapped onto individual PX05 transects at 10-m depth intervals and 0.1° intervals in latitude (PX05 is a meridional transect; Chandler et al. 2021). Salinity was then inferred using a mean temperature-salinity relationship from Argo profiles and objectively mapped at the same resolution for each PX05 transect (Chandler et al. 2021). Following Chandler et al. (2021) and Zilberman et al. (2018), temperature and salinity were linearly interpolated onto the time-mean PX05 transect (called the nominal PX05 transect) using horizontal temperature and salinity gradients from Argo climatology. This enabled mean calculations of conservative temperature, absolute salinity, potential density, dynamic height, and geostrophic velocity along the nominal PX05 route and ultimately provided a near 16-year time-mean description of the currents and water properties within the upper 800 m of the Solomon Sea. Standard deviations were calculated for conservative temperature, absolute salinity, potential density, and geostrophic velocity.

To create the monthly Argo+HR-XBT+Altimetry product, Chandler et al. (2021) utilized a regression relationship between altimetric SLAs and steric height to combine satellite altimetry with the Argo+HR-XBT dataset. SLAs were interpolated onto the PX05 nominal transect and the time-mean SLA was removed to produce the temporal SLA (SLA') for the daily-mean and monthly-mean SLA outputs. Argo+HR-XBT temperature and salinity were used to calculate steric height (h) relative to 800 m (h(z/800)). The removal of the time-mean h at each coordinate (x) and depth (z) then provided the temporal anomaly (h'), and a linear regression was calculated between h' and the 13-day averaged SLA' at each coordinate and depth along the nominal PX05 transect using:

$$h'(z/800)(x) \approx m(x,z) \times SLA'(x) + c(x,z) \quad (1)$$

The gradient and intercept regression coefficients are m and c, respectively.

Once estimates of h' were obtained from applying equation (1) to each monthly-mean SLA, the time-mean h was added back in so that the monthly h could be converted to dynamic height (H) when multiplied by gravity (9.81 m/s^2). Dynamic height calculations consider either 800 m or the ETOPO2 topographic boundary provided by Smith and Sandwell (1997) for the level of no motion, whichever is shallower. The thermal wind relation was used to calculate the geostrophic velocity component normal to the nominal PX05 transect and relative to a level of no motion following:

$$V_g(p) = 1/f \, \delta/\delta x \, [H(p)-H(p_0)] \quad (2)$$

where pressure is represented by p, the pressure at the level of no motion is p_0, and f is the Coriolis parameter. The Argo+HR-XBT+Altimetry dataset provides geostrophic velocity estimates of relatively high temporal (one month) and spatial (0.1° along-transect spacing) resolutions to depths

of 800 m over a period of nearly 16 years (Chandler et al. 2021). The combined Argo+HR-XBT+Altimetry data was utilized to investigate monthly conservative temperature, absolute salinity, and their respective standard deviations, as well as to study monthly geostrophic velocity along the nominal PX05 route. Though Argo+HR-XBT geostrophic velocity encompasses 13°S-1°S, Argo+HR-XBT+Altimetry geostrophic velocity was not defined five degrees within the equator (5°S-0°S).

3. General Characteristics of the Solomon Sea

3.1 Time-Mean Dynamic Height

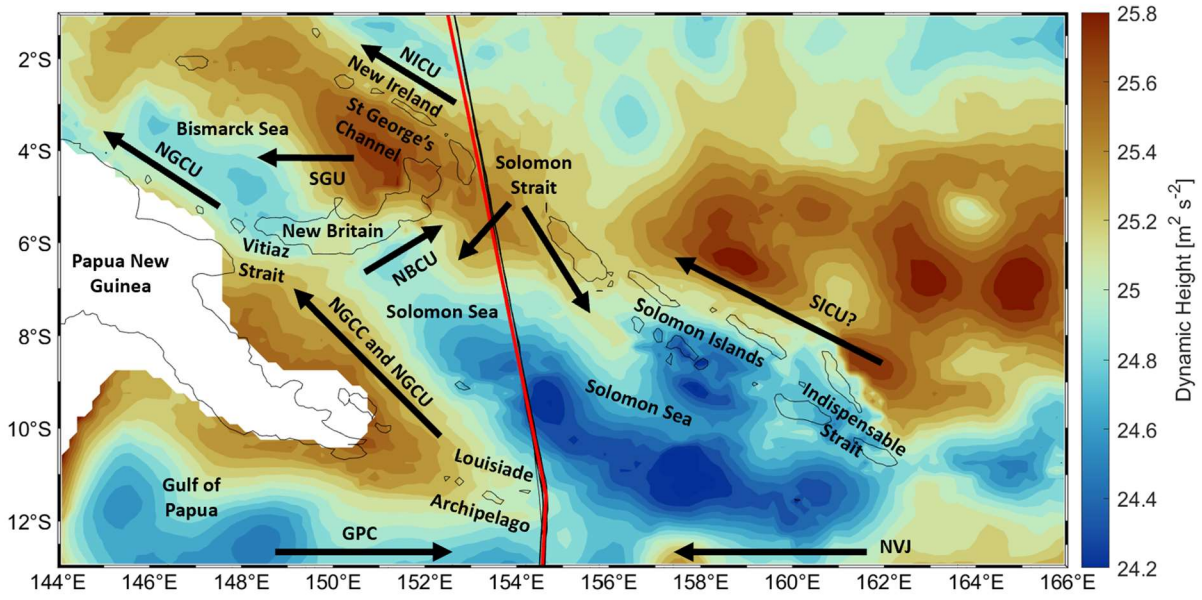

Figure 3. Argo climatological dynamic height of the ocean surface relative to 1975 dbar over the Solomon Sea region with the individual PX05 HR-XBT transects in black and the nominal PX05 HR-XBT transect in red. Interpolation does not acknowledge the islands and a schematic of anticipated currents is overlaid (black arrows, not to scale).

Dynamic height in the Solomon Sea ranged from 24.2 m^2/s^2 to 25.8 m^2/s^2 (Figure 3). The southeast Solomon Sea was dominated by dynamic height near 24.2 m^2/s^2, while greater dynamic height was found along the coasts of southern Papua New Guinea (approximately 25.4 m^2/s^2), the eastern Solomon Islands ($\leq$ 25.8 m^2/s^2), and within the southeast Bismarck Sea ($\leq$ 25.8 m^2/s^2).

Greater dynamic height is a signal of LLWBCs; the islands maintain a pressure gradient which transports the flow along the island boundaries.

3.2 Time-Mean Conservative Temperature

Surface and subsurface waters of the Solomon Sea region demonstrated a deepening mixed layer and narrowing thermocline layers toward the equator (Figure 4). Most variability (provided by standard deviations) occurred at the surface and within the western Solomon Sea near the NGCU. South of the Louisiade Archipelago (13°S) had surface waters of 28°C (standard deviation of 1°C) decrease to 12°C (standard deviation of 0.5°C) by 380 m depth. The 12°C isotherm shoaled to 320 m within the central Solomon Sea (~8°S) and to 290 m near the equator (~1°S), establishing the lower thermocline. The 25°C isotherm (upper thermocline) deepened from near 100 m in the southern Solomon Sea (13°S) to 140 m by the central Solomon Sea (~8°S) and the equator (1°S).

The NGCU was detected through an isothermal dip within the 16°C isotherm (280 m at 10.75°S) and extended to at least the 6°C isotherm (760 m at 11.75°S) as it carried temperatures warmer than the surrounding water through the western Solomon Sea. The 10°C isotherm maintained a relatively steady depth upon exiting the Solomon Strait (370 m at 5.05°S), while the 8°C and 5°C isotherms deepened when crossing Solomon Strait (~500 m at 4.15°S, and ~740 m at 3.85°S respectively). Mean temperature from the Argo+HR-XBT data offered similarities with that from the model study of Melet et al. (2010) who described thermocline layers to reside between 24.0-26.5 kg/m^3.

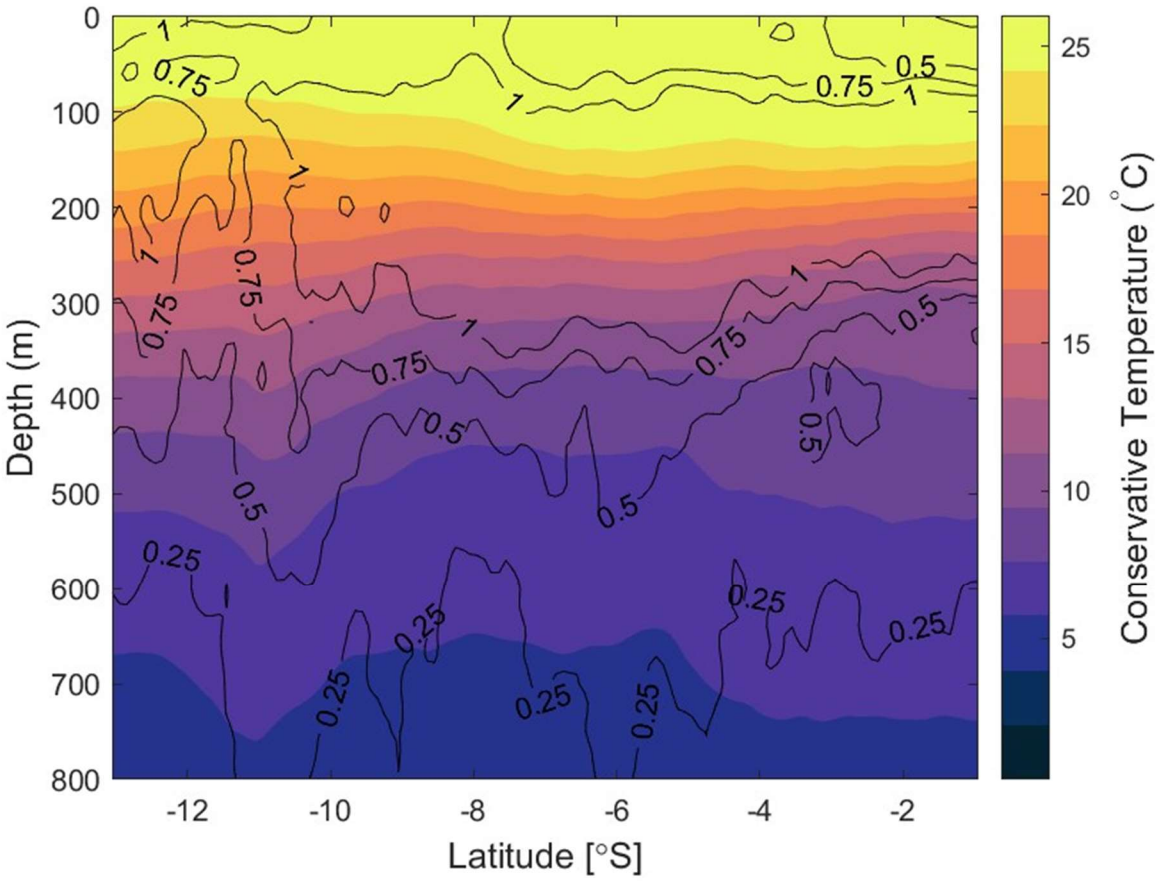

Figure 4. Argo+HR-XBT time-mean conservative temperature (colored contours) and standard deviation (black contours) along the nominal PX05 route from 13°S to 1°S (encompassing the Solomon Sea to the equator).

3.3 Time-Mean Absolute Salinity

Argo+HR-XBT mean salinity illustrated the presence of a subsurface salinity maximum layer throughout the Solomon Sea. This salinity maximum layer narrowed toward the equator (Figure 5). Standard deviations portrayed the most variability at the upper halocline (poleward of 12°S and between approximately 4°S-1°S), as well as in the lower halocline of the central Solomon Sea (~8°S-4°S).

The salinity maximum layer (35.9 g/kg with a standard deviation of 0.05 g/kg) spanned 120-220 m depth south of the Louisiade Archipelago (13°S), constricted near the Solomon Strait inflow to 160-180 m depth (~7°S), and expanded to 130-180 m within the Solomon Strait (~4.45°S). These maximum salinities (35.9 g/kg with a standard deviation of 0.05 g/kg) diminished

near the equator (1.25°S). Surface salinities were near 34.91 g/kg (standard deviations increased near the equator), unless interrupted by saltier waters (35.05 g/kg with a standard deviation of 0.275 g/kg) near the Solomon Strait and New Ireland (~4.85°S-3°S) or a freshwater pool (34.76 g/kg with a standard deviation of 0.25 g/kg) in the central Solomon Sea. The fresh surface waters encompassed 10°S-5.55°S at 0-20 m depth. The NGCU was detected below 290 m (10.85°S) as it carried relatively salty water equatorward towards the Vitiaz Strait and New Britain.

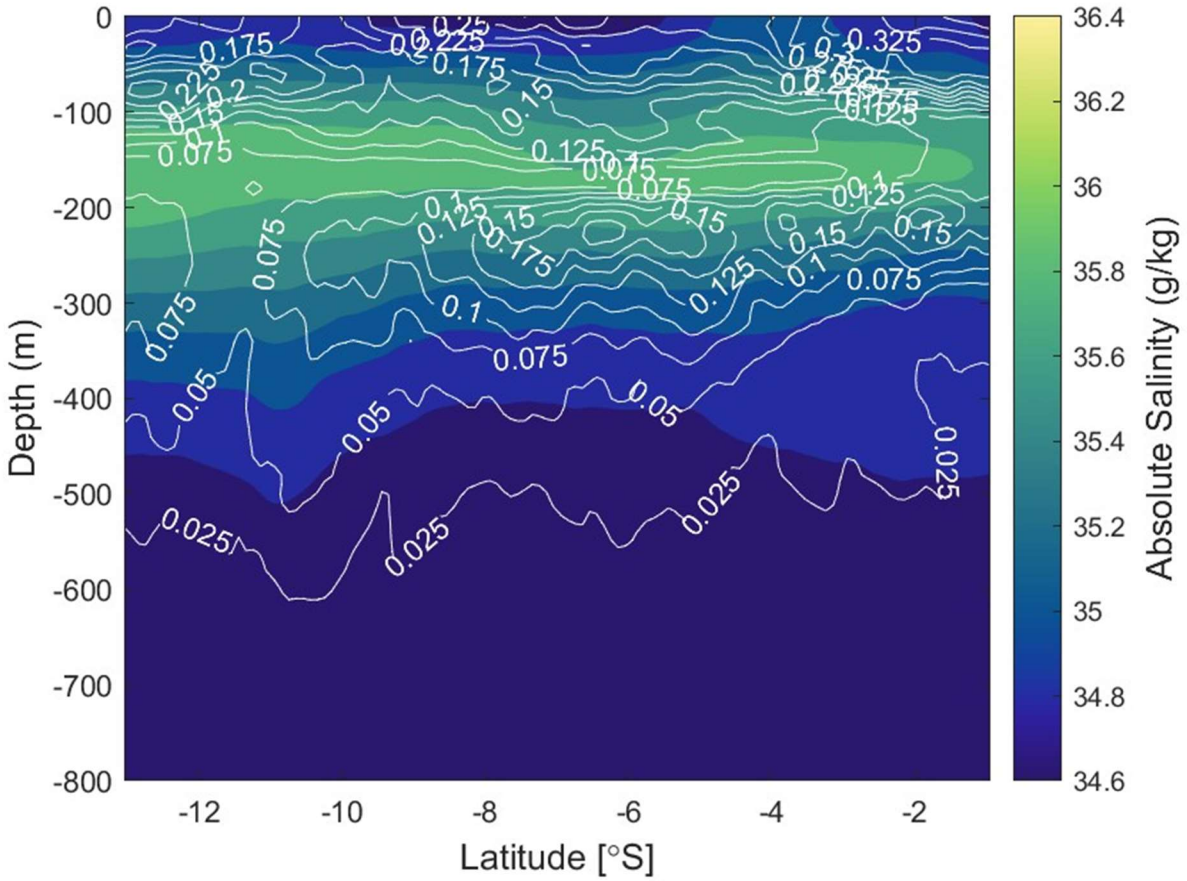

Figure 5. Argo+HR-XBT time-mean absolute salinity (colored contours) and standard deviation (white contours) along the nominal PX05 route from 13°S to 1°S (encompassing the Solomon Sea to the equator).

Anutaliya et al. (2019) suggested that South Pacific Tropical Water (SPTW), identified by a salinity maximum in the upper thermocline layer (the 24.5 kg/m^3 isopycnal), is carried into the Solomon Sea by the NVJ and the GPC. When comparing the southeastern and southwestern Solomon Sea from 0-500m, Anutaliya et al. (2019) found the southeastern Solomon Sea offers a

lower salinity range and the southwestern Solomon Sea offers a greater SPTW signal. Argo+HR-XBT observations exhibit SPTW in the upper thermocline throughout the PX05 nominal transect and offered similar salinity ranges at the southwestern and northeastern edges of the Solomon Sea for the upper 0-800 m.

Germineaud et al. (2016) suggested surface waters host maximum salinity waters east of the Solomon Strait (near 5°S) and that the Solomon Strait acts as an incoming pathway for high-salinity waters to enter the Solomon Sea. Ganachaud et al. (2014) discuss salinity in the surface layer as impacted by rainfall, river runoff, and upwelling. Ganachaud et al. (2014) report rainfall rates of 10 mm/day over the east coast of Papua New Guinea and the south Bismarck Sea, with the remaining Solomon Sea region receiving 8 mm/day (austral summer).

Ganachaud et al. (2014) found salinities of 35.6-35.8 g/kg for the Upper Thermocline Waters (UTW, 24.5 kg/m^3) and 35-35.2 g/kg for the Lower Thermocline Waters (LTW, 26.2 kg/m^3) in the Solomon Sea. Mean salinity from Argo+HR-XBT measurements offered comparable results. Ganachaud et al. (2014) suggested UTW is formed through subduction in the dry and windy eastern center of the South Pacific gyre, whereas the LTW make their way to the Solomon Sea after being subducted northeast of New Zealand. The 24.5 kg/m^3 isopycnal used to define UTW in the study of Ganachaud et al. (2014) corresponds to SPTW in the studies of Anutaliya et al. (2019) and Germineaud et al. (2016). In this study we discuss the 24.5 kg/m^3 isopycnal as SPTW.

3.4 Time-Mean Potential Density

Argo+HR-XBT isopycnals depicted the greatest variability at subsurface levels in the central Solomon Sea (Figure 6). Surface waters of the southern Solomon Sea had potential density anomalies of 22.1 kg/m^3 (with a standard deviation of 0.3 kg/m^3). North of the Louisiade

Archipelago (~10°S), surface potential density anomalies slightly decreased to 21.8 kg/m^3 (with a standard deviation of 0.3 kg/m^3). The upper pycnocline (22.5 kg/m^3 isopycnal with a standard deviation of 0.3-0.5 kg/m^3) gradually deepened towards the equator and sloped to 100 m at 1°S. The lower pycnocline (26.5 kg/m^3 isopycnal with a standard deviation of 0.1 kg/m^3) dipped, giving evidence of the NGCU (400 m depth at 10.85°S), then shoaled to 330 m in the central Solomon Sea and 290 m at the equator. The dips found in the 26.0 kg/m^3 isopycnal (with a standard deviation of 0.1 kg/m^3; 290 m depth at 10.75°S) and the 27.0 kg/m^3 isopycnal (with a standard deviation of 0.1 kg/m^3; 630 m depth at 10.95°S) also suggested the presence of the NGCU.

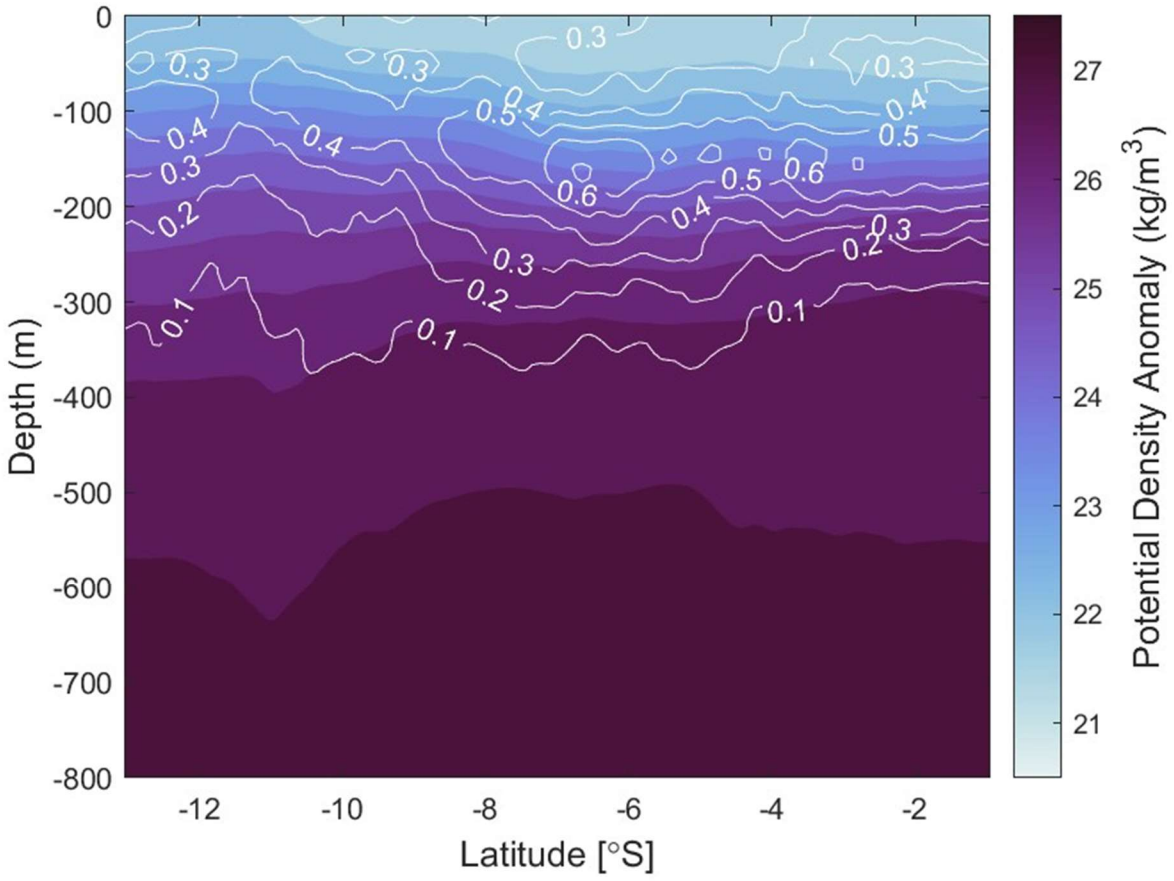

Figure 6. Argo+HR-XBT time-mean potential density anomalies referenced to the surface (colored contours) and standard deviation (white contours) along the nominal PX05 route from 13°S to 1°S (encompassing the Solomon Sea to the equator).

The SPTW, identified by Germineaud et al. (2016) and Anutaliya et al. (2019) by the 24.5 kg/m^3 isopycnal, sat at 160 m throughout the southern and central Solomon Sea (13°S-8°S) then deepened to 190 m near the Solomon Strait (5.95°S) before shoaling to 170 m near the equator (1°S). Germineaud et al. (2016) suggested that the SPTW is found at the upper thermocline level and is composed of two SPTW branches that mix within the southwest Solomon Sea: a high salinity and high oxygen branch that originates in the South Pacific subtropical gyre (20°S) that enters the Solomon Sea through the NVJ, and a second more highly oxygen branch that forms through subduction (30°S) before being carried west by the NCJ, and into the Solomon Sea through the GPC and the NGCU.

South Pacific Subtropical Water (SPSTW, also called Subtropical Mode Water or STMW) was identified by Germineaud et al. (2016) through a density of 25.5-26 kg/m^3 and a thermostad typically associated with mode waters. SPSTW originates north of the Tasman Sea and northeast of New Zealand. Density estimates using Argo+HR-XBT data found the SPSTW spans 250-300 m depth south of the Solomon Sea (13°S) and 200-230 m at the equator (1°S).

Together, the SPTW and SPSTW makeup Subtropical Lower Water (SLW, Germineaud et al. 2016). According to Argo+HR-XBT densities, SLW covered 160-300 m in the southern Solomon Sea (13°S), 160-320 m within the central Solomon Sea (8°S), and 170-290 m at the equator (1°S). SLW encompassed lower and upper thermocline levels.

Subantarctic Mode Water (SAMW, 26.5-27 kg/m^3) was detected by Argo+HR-XBT measurements between 380-570 m in the southern Solomon Sea (13°S), 320-500 m in the central Solomon Sea (~8°S) and between 290-550 m near the equator (1°S). The upper level of the SAMW (26.5 kg/m^3 isopycnal) gradually shoaled within the Solomon Sea, whereas the lower layer of the

SAMW (27 kg/m^3 isopycnal) had a sharper drop near the Solomon Strait (~4.5°S). SAMW is formed through subduction north of the Antarctic Circumpolar Current (Germineaud et al. 2016).

Germineaud et al. (2016) assigned Antarctic Intermediate Water (AAIW) densities of 26.9-27.4 kg/m^3 based on observations of its salinity minimum (< 34.6 g/kg) and oxygen maximum (~150–200 μmol/kg). AAIW forms between 50°S-60°S and is subducted between 170°W and the Drake Passage (Germineaud et al., 2016; Ganachaud et al., 2014). AAIW is brought to the NGCU by the GPC from the Coral Sea (Germineaud et al., 2016). Argo+HR-XBT densities found AAIW to reside deeper than 500 m in the southern Solomon Sea (poleward of 10°S), near 440 m within the central and northern Solomon Sea (10°S-5°S) and at approximately 480 m depth near the Solomon Strait (5°S-1°S) and equatorward. Germineaud et al. (2016) and Lukas et al. (1996) agree that the lower NGCU carries AAIW equatorward, though Germineaud et al. (2016) found the AAIW signal to be lost to high salinities near the Vitiaz and Solomon Straits.

3.5 Time-Mean Temperature-Salinity (TS) Plot

Conservative temperature within the Coral and Solomon Seas ranged from approximately 4°C to 32°C while absolute salinity ranged from approximately 34.6 g/kg to 36.3 g/kg (Figure 7). Argo+HR-XBT data suggested waters above the thermocline warmed near the equator and waters below the thermocline were saltier near the equator. SPTW and AAIW were identified by their salinity maximums and minimums, respectively.

Although Germineaud et al. (2016) observed an increase in salinity between the southern NGCU (near the Louisiade Archipelago) and the Solomon Strait, they emphasized an increase in salinity along an east-west direction rather than a north-south direction in the Solomon Sea. Germineaud et al. (2016) observed maximum salinities east of the Solomon Strait and high salinities within the southeast Solomon Sea (carried by the SEC and NVJ respectively), and fresher

waters within the western Solomon Sea and the Vitiaz Strait. Germineaud et al. (2016) offered the east-west salinity differences within the southern Solomon Sea are products of oceanic pathways, as the southeastern Solomon Sea receives SPTW from the NVJ and the southwestern Solomon Sea receives SPTW from the GPC. The branch carried to the Solomon Sea by the NVJ (characterized as high salinity and high oxygen) forms through subduction within the subtropical central South Pacific, while the branch of the SPTW carried to the GPC by the NCJ (characterized as fresher) is formed through subduction at 30°S.

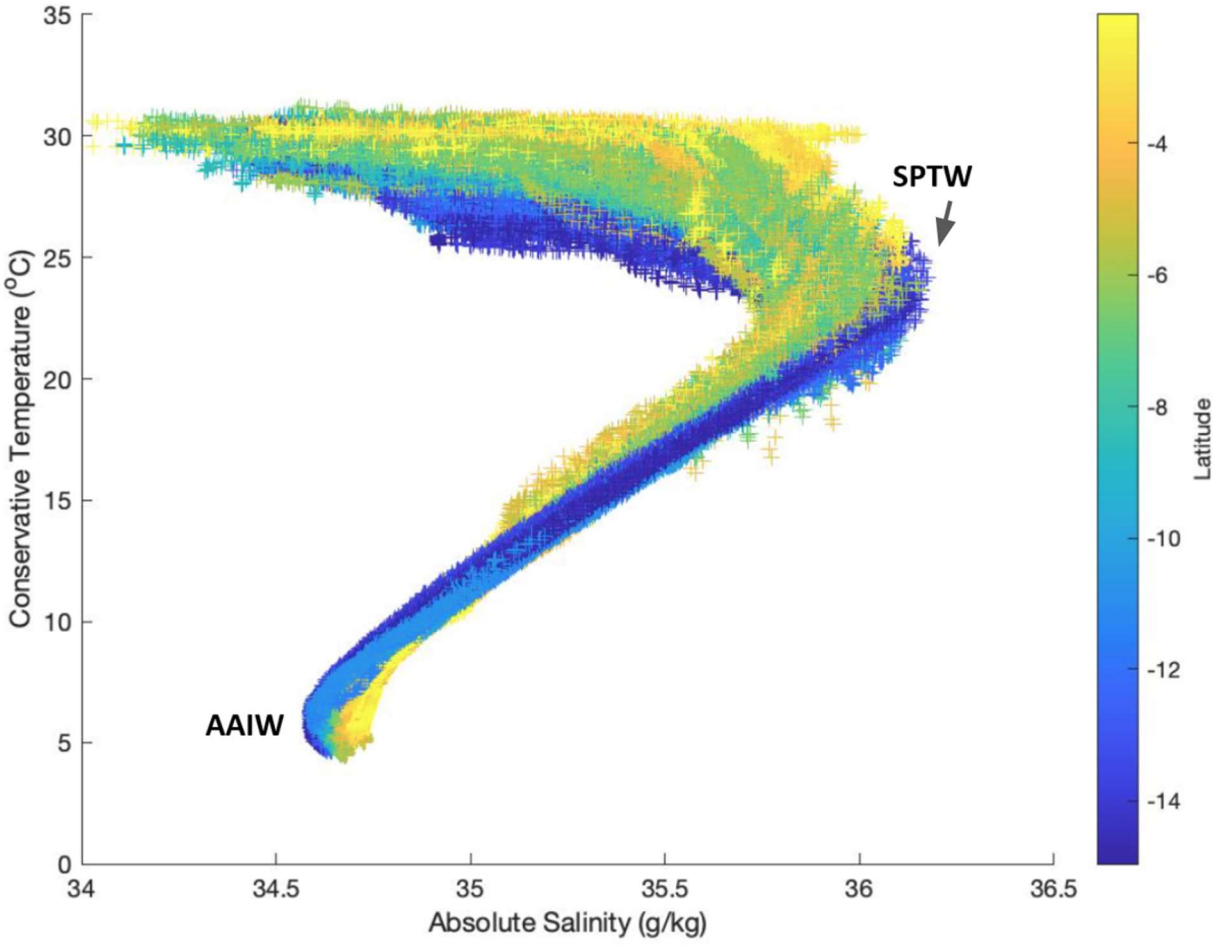

Figure 7. Argo+HR-XBT temperature-salinity (TS) characteristics of the upper 800 m in the Coral and Solomon Seas (15°S-2°S).

3.6 Time-Mean Geostrophic Velocity

Time-mean geostrophic velocities varied in speed and direction throughout the transect (Figure 8). The weak westward velocities (indicated by negative values) of the NVJ (13°S to 11.65°S at surface levels) weakened with depth as they approached the Solomon Sea. Ganachaud et al. (2014) described the NVJ's reach as "broad but shallow." Argo+HR-XBT derived geostrophic velocities agree that the strongest portions of the NVJ are shallow (0.12 m/s with a standard deviation of 0.3 m/s in the upper 60 m and 0.05 m/s with a standard deviation of 0.1 m/s by 160 m), since currents below 160 m reduced to 0.01 m/s (with a standard deviation of 0.1 m/s).

The GPC had maximum velocities near 0.19 m/s (with a standard deviation of 0.2 m/s) from 200-370 m depth, and though the surface GPC encompassed 11.45°S to 10.85°S, the subsurface GPC extended to 12.45°S. The GPC decreased to 0 m/s at 640 m. The NGCU/NGCC system resided near the surface from 10.85°S to 8.55°S while the NGCU broadened to at least 8°S at 400 m depth. The maximum velocities (0.26 m/s with a standard deviation of 0.2-0.1 m/s west) of the NGCU resided within 170-270 m depth (10.35°S); the NGCU weakened to 0.15 m/s (with a standard deviation of 0.1 m/s) at 430 m and to 0.12 m/s (with a standard deviation of 0.4 m/s) at the surface. The northern NGCU/NGCC core flowed at speeds of 0.2 m/s with standard deviations from 0.1-0.5 m/s. Argo+HR-XBT mean geostrophic velocity supports the NGCU being fed by the GPC since their maximum velocities align in depth. Ganachaud et al. (2014) suggested the GPC's core is near 400 m, and Germineaud et al. (2016) suggest the NGCU core is at 500 m depth, but geostrophic velocity calculations with Argo+HR-XBT observations portrayed the central cores of the GPC and NGCU higher in the water column. Maximum velocities of the NGCU were slightly greater than Melet et al. (2010), who modeled velocities at 20 cm/s between 100-300 m.

At the surface, the central Solomon Sea was dominated by eastward velocities as great as 0.42 m/s (with a standard deviation of 0.6 m/s). These eastward velocities (between 8.35°S to 6.75°S) decreased to zero by 150-250 m and partially gave way to weakened westward velocities with depth. Previous studies discussed the common occurrence of eddies within the eastern and southern Solomon Sea (Anutaliya et al. 2019, Ganachaud et al. 2014, Melet et al. 2010). A high variability would suggest the central Solomon Sea's eastward velocities were also due to the presence of eddies. Argo+HR-XBT calculations provided a standard deviation of 0.3-0.6 m/s dependent on depth. The low variability and persistence over the long (near 16-year) observational period suggests the central Solomon Sea's eastward velocities to be more permanent than eddies.

The Solomon Strait to the equator (approximately 7°S to 1°S), experienced a series of flow reversals. Among these reversals was the Solomon Strait inflow (5.95°S to 4.25°S) consisting of westward surface velocities up to 0.38 m/s (with a standard deviation of 0.6 m/s around 5.35°S). Though part of the flow below the Solomon Strait inflow remained weakly westward at lower depths, the NBCU was found under the Solomon Sea inflow (the NBCU spans 5.35°S-4.45°S). The greatest speeds of the NBCU were found between 260-450 m depth and flowed with a maximum velocity of 0.24 m/s eastward (with a standard deviation of 0.1-0.3 m/s). The NBCU's speeds decreased to zero by 130 m and 680 m depth. It is unclear if the slight eastward velocities (0.14 m/s with a standard deviation of 0.1 m/s) from 300-520 m upon exiting the Solomon Strait (near 4°S) were more closely related to the NBCU or to the strong (0.33 m/s with a standard deviation of 0.6 m/s) eastward velocities that resided above.

Alberty et al. (2019) detected a flow centered near 250 m exiting the Solomon Strait. Melet et al. (2010) described the NBCU as 10 km south of New Britain with a core modelled at 60 cm/s near 230 m. This places the observation of Alberty et al. (2019) and the model velocities of Melet

et al.'s (2010) NBCU higher in the water column than the Argo+HR-XBT observations. Alberty et al. (2019) also suggested that the westward Solomon Strait inflow was slower than the NBCU. Mean Argo+HR-XBT observations suggested the Solomon Sea inflow is slower than the NBCU when directly above the NBCU, however the Solomon Sea inflow south of the NBCU is faster than the NBCU and the inflow to the north is near the same magnitude of the NBCU.

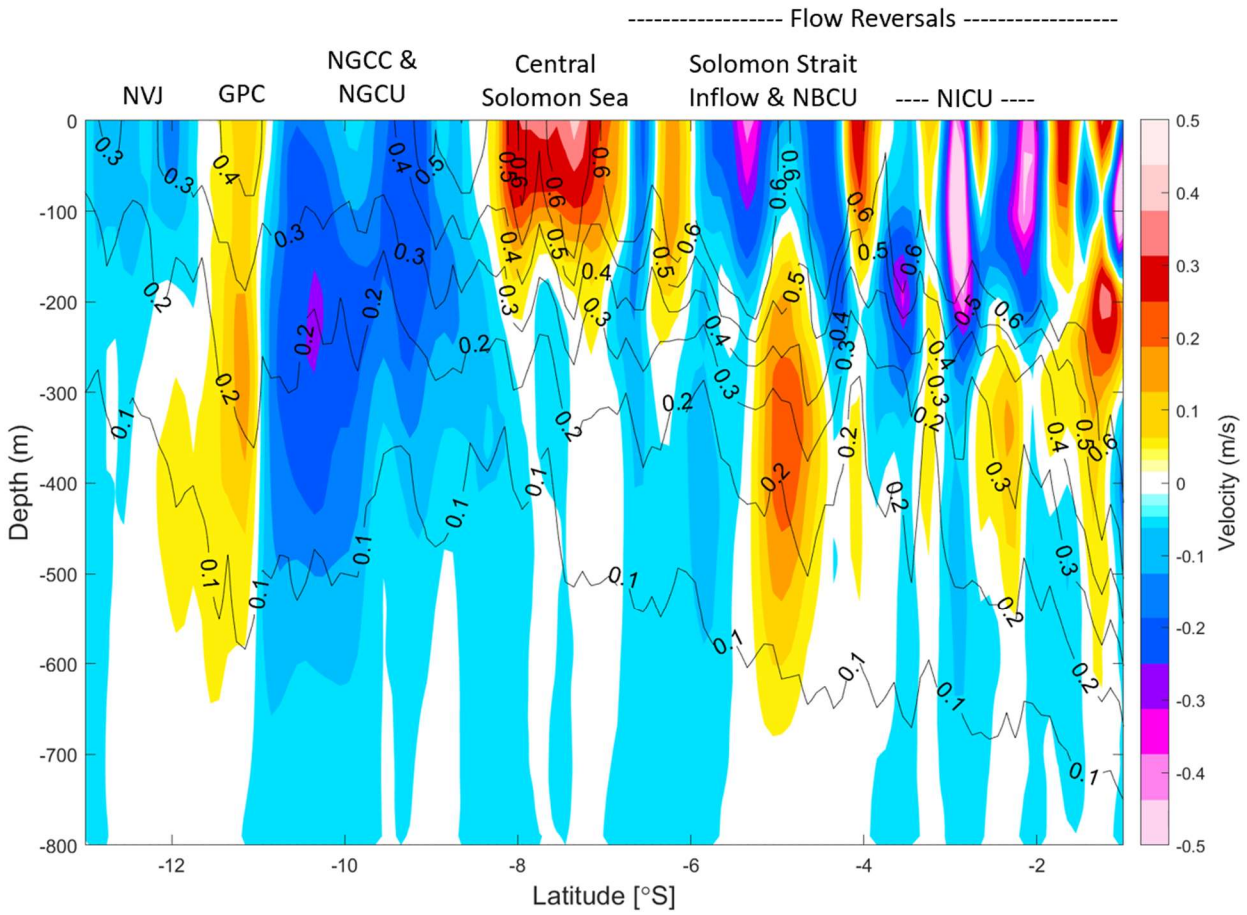

Figure 8. Argo+HR-XBT time-mean geostrophic velocity (m/s) of the upper 800 m along the nominal PX05 route from 13°S to 1°S (encompassing the Solomon Sea to the equator). Positive values (warm colors) represent eastward flow while negative values (cool colors) represent westward flow. Standard deviations (black contours) range from 0.1 m/s to 0.6 m/s.

A westward subsurface core of 0.31 m/s (with a standard deviation of 0.5-0.6 m/s) was found near 200 m depth beside New Ireland (3.45°S). North of weak eastward velocities (≤ 0.13 m/s with a standard deviation ranging 0.1-0.6 m/s persistent to 480 m depth at 3.25°S) were two

powerful westward surface flows also near New Ireland. The first (~3°S) flowed at speeds of 0.55 m/s (with a standard deviation of 0.5-0.6 m/s) in the upper 180 m and weakened to 0.1 m/s (with a standard deviation of 0.3 m/s) by 290 m. The second (2.15°S) had maximum velocities of 0.5 m/s (with a standard deviation of 0.6 m/s) from 40-100 m depth and was disrupted by an eastward flow at lower depths.

Neither of the westward flows near New Ireland fully fit into previous descriptions of the NICU. The flow at 3.45°S off the coast of New Ireland agrees more closely with the 230 m-depth placement of the NICU by Melet et al. (2010) and Butt and Lindstrom (1994), yet both studies suggested the NICU reached speeds near 0.6 m/s (as did Alberty et al. 2019) which mean Argo+HR-XBT geostrophic velocities did not provide. The surface flow near 3°S offered speeds closest to 0.6 m/s, however Argo+HR-XBT geostrophic velocities placed the mean maximum velocities of this westward flow at the surface. Instead of nearing 0.6 m/s near 230 m, the westward velocities at 3°S were 0.45 m/s (with a standard deviation of 0.4 m/s) at 230 m depth and 0.12 m/s (with a standard deviation of 0.3 m/s) at 280 m depth. Furthermore, the westward surface flow near 2°S reduced to 0.41 m/s (with a standard deviation of 0.6 m/s) by 170 m –a speed and depth placement slower and shallower than the 0.6 m/s and 230 m core noted by others (Melet et al. 2010; Butt and Lindstrom 1994; Alberty et al. 2019). Despite these differences, it is likely that two or all of these westward flows do form the NICU. In their model, Melet et al. (2010) commented on the NICU splitting into two branches at 2°S, with the western branch pouring into the Bismarck Sea to rejoin the NGCU and the eastern branch heading directly equatorial towards the EUC. The NICU-EUC connection establishes a direct route for thermocline waters to travel from the Solomon Sea to the equator.

Argo+HR-XBT measurements demonstrated an eastward flow (2.65°S) at speeds of 0.22 m/s (with a standard deviation of 0.6 m/s) between the surface and 70 m interrupting the westward surface velocities, as well as a subsurface eastward flow centered near 340 m depth flowing at speeds of 0.16 m/s (with a standard deviation of 0.3 m/s) at 2.35°S (beneath the NICU marking in Figure 8). This subsurface flow may be the same flow detected by Butt and Lindstrom (1994) at 240 m depth near 2°S. Numerous reversals occurred across the nominal PX05 transect in the upper 200 m north of the NICU (from south to north): an eastward maximum of 0.30 m/s (with a standard deviation of 0.6 m/s) reduced to zero near 200 m (1.65°S), then a westward flow of 0.19 m/s (with a standard deviation of 0.6 m/s) reduced to zero at the surface and 150 m (1.35°S), next an eastward flow with a maximum of 0.37 m/s (with a standard deviation of 0.6 m/s) weakened with depth (1.25°S), and lastly strong westward velocities up to 0.54 m/s (with a standard deviation of 0.6 m/s; 1.05°S) spanned from the surface to at least 170 m. At 1.25°S a subsurface eastward core persisted near 210 m depth with speeds of 0.39 m/s (with a standard deviation of 0.6 m/s), which reduced to 16 m/s (with a standard deviation of 0.5 m/s) by 320 m, and to zero by 620 m depth.

3.7 Time-Mean Depth-Integrated Geostrophic Velocity

The time-mean depth-integrated velocity over the upper 800 m (Figure 9, relative to 800 m) included several shifts in direction and magnitude in and around the Solomon Sea (13-1°S). The NVJ flowed at speeds ≤ 38 m^2/s westward. The GPC (12.35-11.05°S) divided into two streams at the Louisiade Archipelago: the southern flow reached maximum depth-integrated velocities of 43.83 m^2/s eastward, and the northern flow reached maximum depth-integrated velocities of 78.65 m^2/s eastward. The NGCU and NGCC similarly broke into two streams: the southern peak reached up to 112 m^2/s while the northern peak reached up to 75.61 m^2/s. The central Solomon Sea experienced depth-integrated velocities up to 56.04 m^2/s between 8.15°S-6.85°S. Flow reversals

were present near the Solomon Strait and equatorward. The westward flow near 6.5°S reached ≤ 46.13 m^2/s and its neighboring eastward flow reached up to 35.81 m^2/s. The Solomon Strait inflow entered the Solomon Sea at ≤ 42.15 m^2/s and the underlying NBCU exited the Solomon Strait at ≤ 87.83 m^2/s. Flow reversals were evident east of New Ireland with depth-integrated velocities (from south to north) of: ≤ 47.91 m^2/s westward, ≤ 62.4 m^2/s eastward, ≤ 61.8 m^2/s westward, ≤ 41.08 m^2/s eastward, and ≤ 136.1 m^2/s westward near 2.95°S. It is likely the first westward flow after the NBCU is part of the Solomon Strait inflow. Figure 9 depicts the strongest westward flow as the NICU, however the NICU may be composed of a multitude of westward flows (see Figure 8). The subsequent flow reversals (south to north) flowed up to 13.29 m^2/s eastward and 66.78 m^2/s westward, and the flow near 1°S was at least 96 m^2/s eastward.

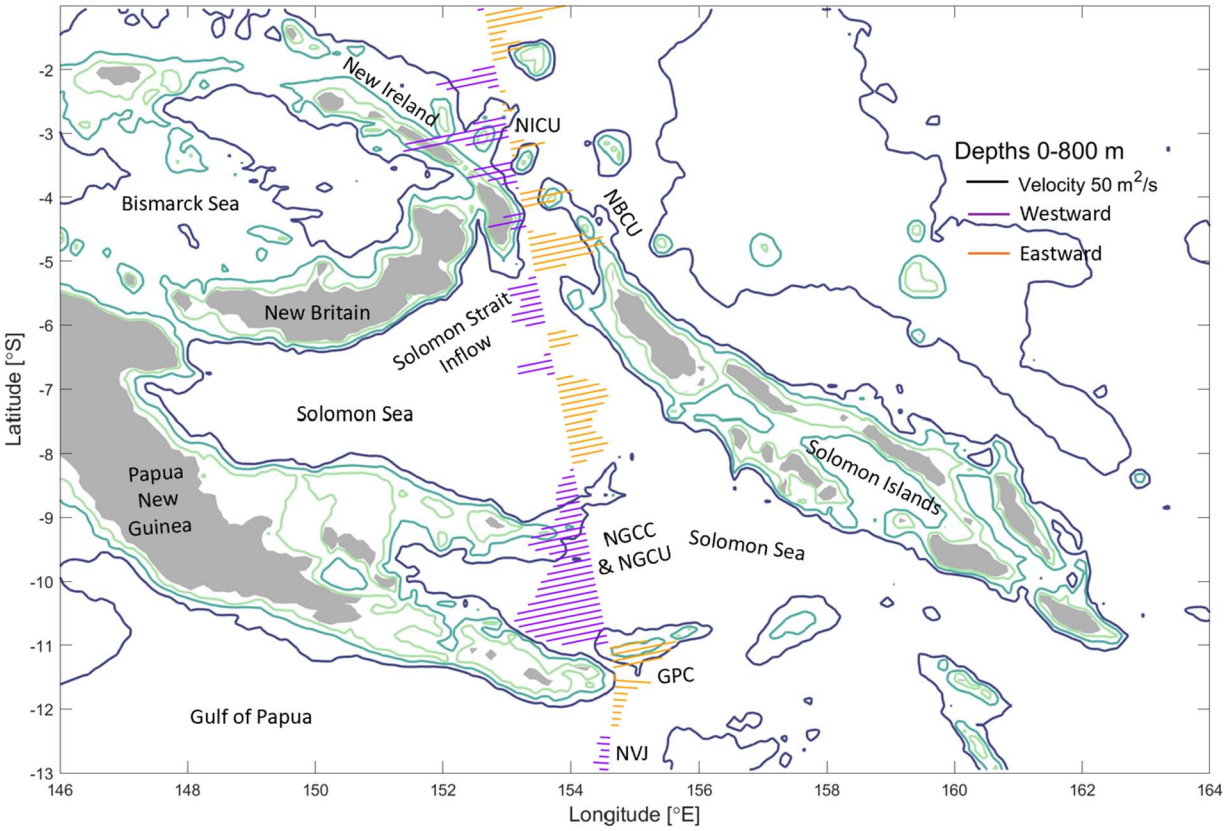

Figure 9. Argo+HR-XBT time-mean velocity integrated of the upper 800 m (relative to 800 m) across 13°S -1°S on the nominal PX05 transect. Land masses are depicted in gray, alongside the 200 m isobath (green), 1000 m isobath (blue), and 2000 m isobath (purple).

Chandler et al. (2021) considered monthly (Argo+HR-XBT+Altimetry) depth-integrated (0-800 m) geostrophic velocity from 2005-2019 normal to the nominal PX05 transect (excluding five degrees north and south of the equator). Their assessment provided similar magnitudes of the NGCU (100-200 m^2/s westward) and the central Solomon Sea (0-100 m^2/s eastward) and demonstrated three flow reversals near the Solomon Strait. Chandler et al. (2021) suggested flow reversals amongst transects are likely a product of eddies.

Depth-integrated velocity of the upper 150 m (Figure 10, relative to 150 m) offered geospatial shifts in currents when compared to the depth-integrated velocities over the full 800 m. The 150 m limit was selected so that surface and subsurface cores would remain primarily in-tact during investigations (see Figure 8). The NVJ covered 13°S-11.75°S in the upper 150 m with depth-integrated velocities that reached nearly a third ($\leq$ 12.78 m^2/s) of the 0-800 m depth-integrated geostrophic velocity. Coinciding with the NVJ's greater northward reach, the GPC's two streams were only present from 11.65-10.95°S. The southern GPC stream reached a maximum depth-integrated velocity of 6.88 m^2/s, and the northern GPC stream reached a maximum depth-integrated velocity of 19.03 m^2/s. The NGCU/NGCC system also maintained its two-stream feature: the southern stream reached 28 m^2/s and the northern stream reached 30.13 m^2/s. The NGCC's spatial extent along the nominal PX05 transect reduced slightly compared to the 0-800 m investigations and gave way to the eastward depth-integrated velocities of the central Solomon Sea. The central Solomon Sea held depth-integrated velocities up to 42.94 m^2/s between 8.45-6.75°S. The westward flow near 7°S and eastward flow near 6.5°S had depth-integrated velocities up to 20.88 m^2/s and 26.96 m^2/s, respectively. With no detection of the NBCU in the upper 150 m, the Solomon Strait inflow (depth-integrated velocities $\leq$ 41.77 m^2/s westward) fully covered the Solomon Strait (10.77-11.2°S). Flow reversals neighboring New Ireland (south to north) had

depth-integrated velocities of: ≤ 35.97 m^2/s eastward, ≤ 15.02 m^2/s westward, ≤ 12.45 m^2/s eastward and ≤ 75.57 m^2/s westward (~3°S). The NICU may be comprised of more than one westward stream (see Figure 8). The final flow reversals along the nominal PX05 transect include (south to north): ≤ 11.91 m^2/s eastward, ≤ 56.41 m^2/s westward, ≤ 33.61 m^2/s eastward, ≤ 16.11 m^2/s westward, ≤ 23.82 m^2/s eastward, and ≤ 20.37 m^2/s westward.

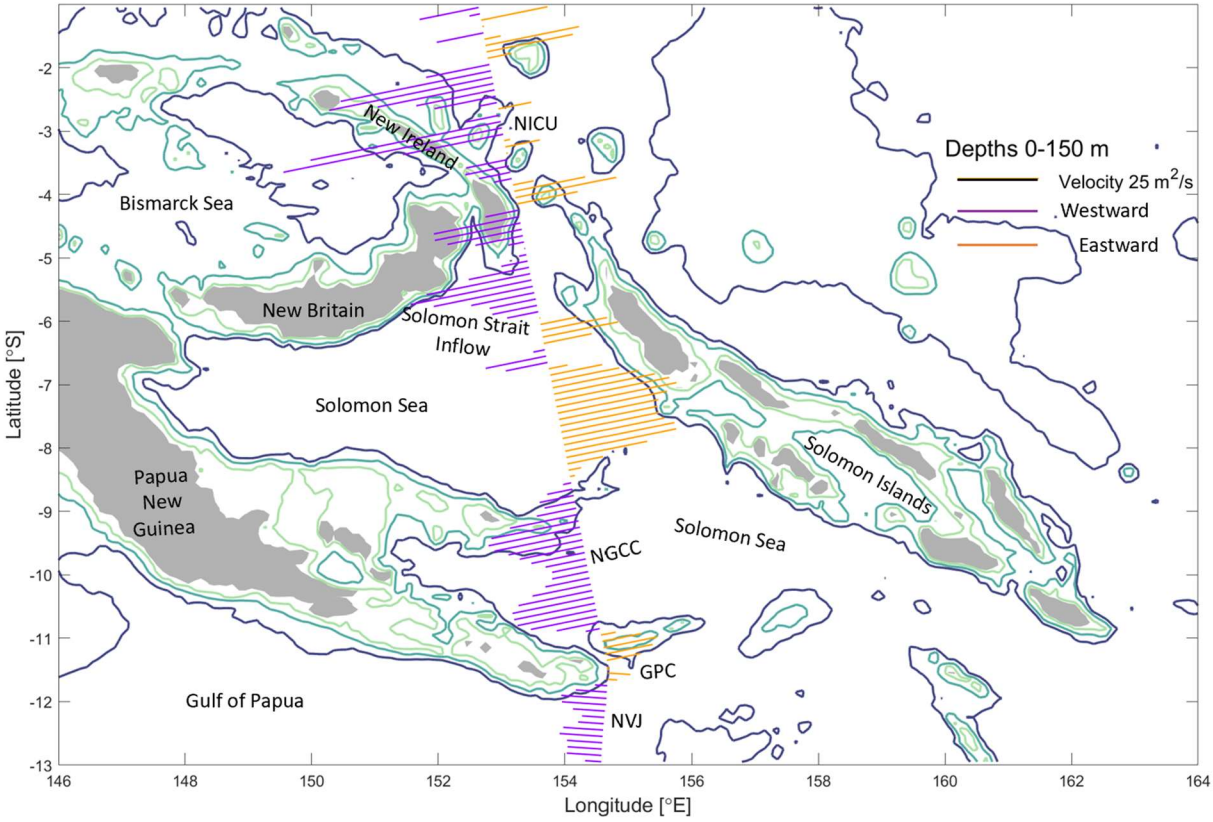

Figure 10. Argo+HR-XBT time-mean depth-integrated velocity of the upper 150 m (relative to 150 m) across 13°S -1°S on the nominal PX05 transect. Land masses are depicted in gray, alongside the 200 m isobath (green), 1000 m isobath (blue), and 2000 m isobath (purple). Note the change in scale.

The depth-integrated velocity from 160-800 m depth (Figure 11, relative to 800 m) illustrated the NVJ (≤ 16.01 m^2/s) residing poleward of 12.45°S and the GPC (southern stream ≤ 44.31 m^2/s and northern stream ≤ 79.24 m^2/s) spanning 12.35°S-11.05°S. The southern maximum of the NGCU flowed alongside Papua New Guinea with depth-integrated velocities ≤ 120.28 m^2/s and the northern maximum of the NGCU with depth-integrated velocities ≤ 74.1 m^2/s (together

encompassing 10.95-8.25°S). Eastward depth-integrated velocities (≤ 37.93 m^2/s) in the central Solomon Sea covered 8.15°S-6.85°S. The westward flow near 6.65°S and eastward flow near 6.25°S had depth-integrated velocities ≤ 49.65 m^2/s and 31.63 m^2/s, respectively. The Solomon Sea inflow (5.42°S-4.25°S) entered the Solomon Sea with a maximum depth-integrated velocity of 38.85 m^2/s south of the NBCU and 52.21 m^2/s north of the NBCU. The NBCU (5.25°S-24.9°S) exited the Solomon Strait with maximum depth-integrated velocities of 105.21 m^2/s. The maximum depth-integrated velocities of the flow reversals east of New Ireland were as follows (south to north): 41.74 m^2/s eastward, 87.27 m^2/s westward, 34.72 m^2/s eastward, 132.9 m^2/s westward (labeled NICU in Figure 11. See Figure 8 for detail on the NICU), 13.17 m^2/s eastward, and 60.1 m^2/s westward. Near 1°S the eastward depth-integrated velocities reached 84.53 m^2/s.

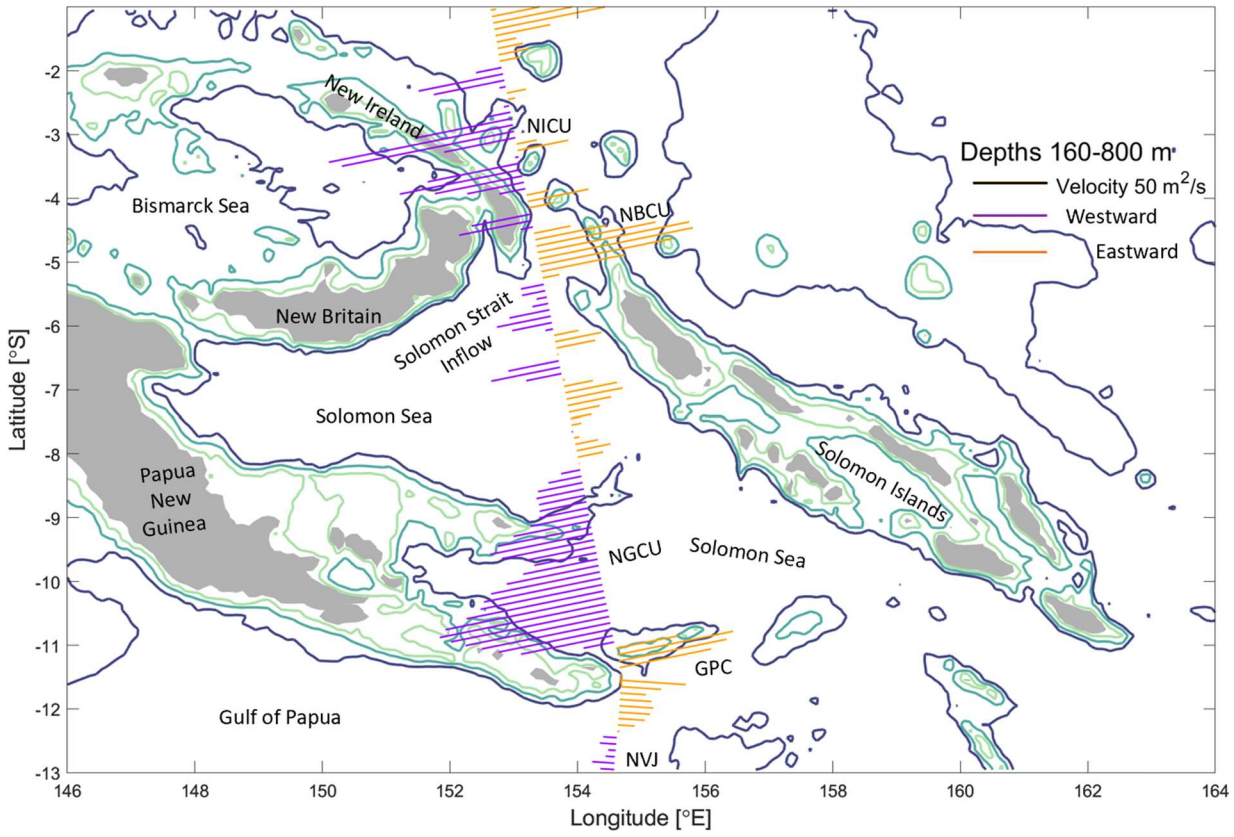

Figure 11. Argo+HR-XBT time-mean depth-integrated velocity of 160-800 m depth (relative to 800 m) across 13°S -1°S on the nominal PX05 transect. Land masses are depicted in gray, alongside the 200 m isobath (green), 1000 m isobath (blue), and 2000 m isobath (purple). Note the change in scale.

The depth-integrated flows from 0-150 m and 160-800 m had similar directions normal to the PX05 transect near the Solomon Sea (Figure 12). Exceptions included near 12°S in the NVJ and GPC interface and near the Solomon Strait (~5°S). Generally the magnitude of the depth-integrated velocities within the upper 150 m were less than 160-800 m (likely a function of speed and layer thickness), however there were few exceptions. For example, the surface and subsurface flows of the NVJ were between 10-20 m^2/s and the upper 150 m of the central Solomon Sea were greater in magnitude than the 160-800 m depth-integrated velocities. Argo+HR-XBT data suggested the greatest depth-integrated velocities are the GPC (reaching a peak of 85 m^2/s at 11.15°S), the southern maximum of the NGCU (reaching a peak of 122.72 m^2/s at 10.35°S), the NBCU (reaching a peak of 107.34 m^2/s at 4.95°S), the NICU (reaching a peak of 135.60 m^2/s at 2.85°S) and the eastward flow at 1.25°S (reaching a peak of 111.78°S m^2/s at 1.25°S).

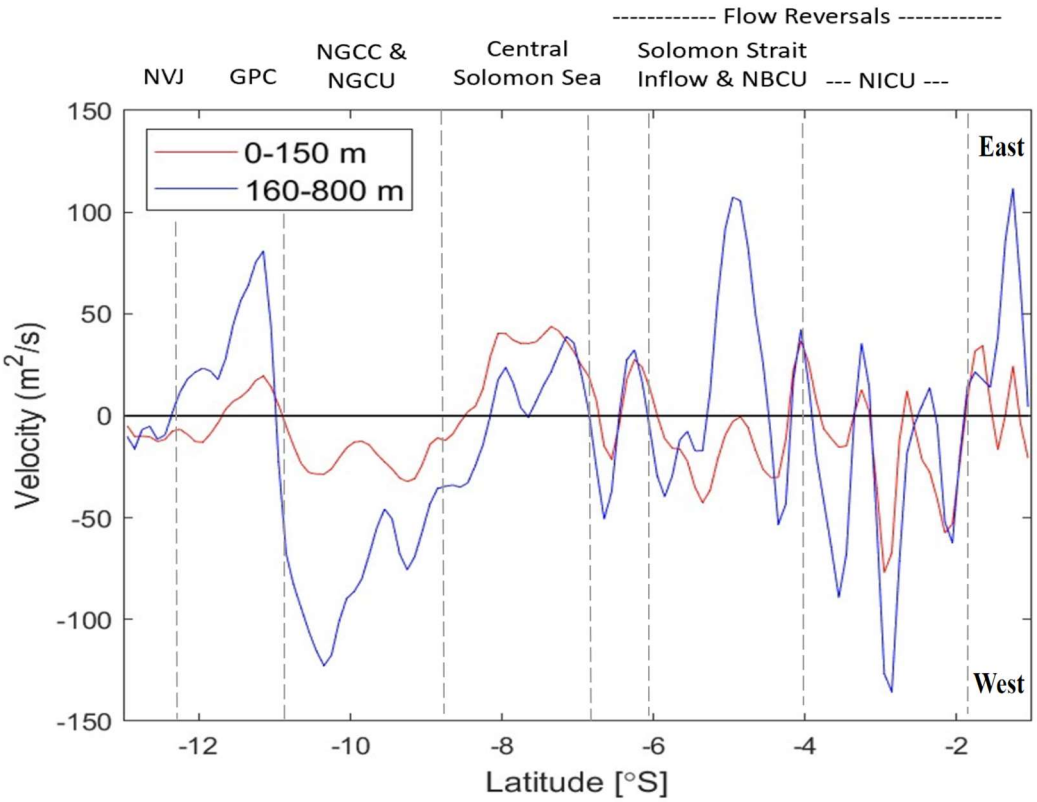

Figure 12. Argo+HR-XBT depth-integrated velocity of 0-150 m (red) and 160-180 m (blue) along the nominal PX05 route from 13°S-1°S (encompassing the Solomon Sea to the equator). Negative velocities indicate a westward flow while positive values indicate eastward flow.

4. Monthly Properties within the Solomon Sea

4.1 Monthly Mean Conservative Temperature

In austral summer (November-January), surface temperatures along the nominal PX05 route reached up to 30.2°C (with a standard deviation of 0.5°C; Figure 13). The mixed layer deepened through austral fall (ranging 28.6°C and 30°C, both with a standard deviation of 0.5°C in April) and the high temperatures found in austral summer persisted until the start of austral winter (May). Surface temperatures of the southern Solomon Sea lowered through the remainder of austral winter into austral spring (surface waters now ranged from 26°C to 29.8°C, both with a standard deviation of 0.5°C in October). In March and July the NGCU was not well-defined by isothermal dips, yet in June and the remaining months the NGCU could be detected near 240 m or below.

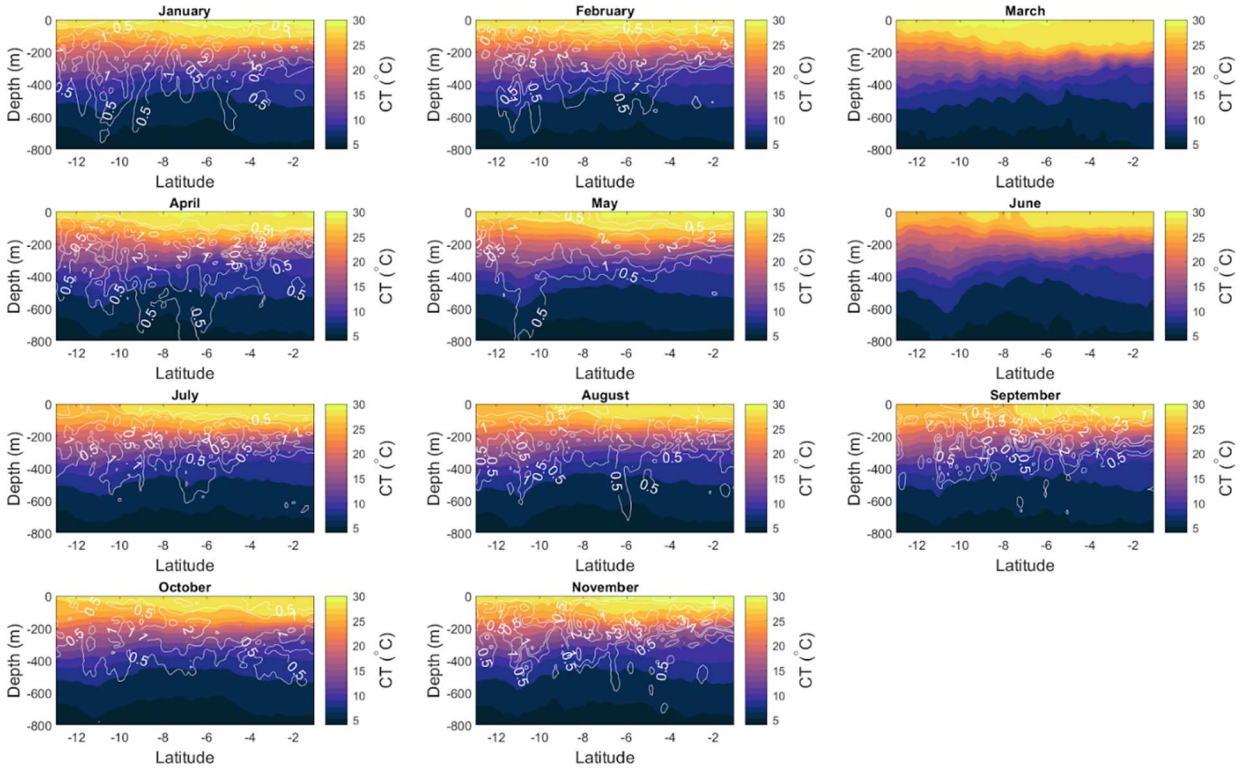

Figure 13. Argo+HR-XBT+Altimetry derived monthly conservative temperature (CT) with standard deviations (white) along the nominal PX05 route from 13°S-1°S (encompassing the Solomon Sea to the equator).

4.2 Monthly Mean Absolute Salinity

SPTW (35.6-35.8 g/kg) resided at the thermocline level throughout the Solomon Sea year-round with slight variation. Standard deviations from Argo+HR-XBT+Altimetry data were most variable at the surface levels and in the salinity signal of the NGCU (Figure 14).

In austral summer (November-January), the Argo+HR-XBT+Altimetry dataset located the highest salinities (36.0 g/kg with a standard deviation of 0.1 g/kg) within the thermocline depths poleward of 10°S, and the freshest water (34.5 g/kg with a standard deviation of 0.2 g/kg) over the surface of the southern (November) and central (January) Solomon Sea. The Solomon Strait inflow introduced relatively salty surface waters (34.9 g/kg with a standard deviation of 0.2 g/kg) into the Solomon Sea and the deeper NGCU carried relatively salty waters (34.8 g/kg with a standard deviation of 0.1 g/kg near 515 m) equatorward.

March was the saltiest month in austral fall (February-April). Argo+HR-XBT+Altimetry data measured high-salinity surface waters (≥ 35 g/kg) equatorward of the NGCU and NGCC (northward of 9°S). Unlike February and April, March was characterized by maximum salinities (36.1 g/kg) near the Solomon Strait (6.25°S, and northward of 4°S). Argo+HR-XBT+Altimetry data portrayed April as the freshest month within austral fall. April held fresh surface waters (34.3 g/kg with a standard deviation of 0.1 g/kg) over the central Solomon Sea (~10°S-6°S) and Solomon Sea inflow of 34.9 g/kg (with a standard deviation of 0.1 g/kg). The isohaline dips of the NGCU were clearly defined in April but not February or March.

Anutaliya et al. (2019) observed low salinity waters in March-April and attributed the low salinity to anonymously fresh water brought in by a weakened Solomon Sea inflow. Because the Solomon Sea inflow is believed to confine to the northern and eastern sides of the basin, Anutaliya

et al. (2019) used the seasonal salinity cycle observed at the upper thermocline level (24.5 kg/m^3) within the eastern Solomon Sea to propose a rapid increase of equatorward flow in April.

In austral winter (May-July), Argo+HR-XBT+Altimetry data detected the isohaline dips of the NGCU to at least 520 m depth as saltier waters (34.8 g/kg with a standard deviation of 0.1 g/kg) were brought towards the northern Solomon Sea. In June, high salinities of 36.0 g/kg were confined poleward of the NGCU (11.45°S), and the surface waters south of the Solomon Strait were slightly saltier than May or July (34.9 g/kg, compared to 34.7 g/kg and a standard deviation of 0.1 g/kg respectively). The Solomon Strait inflow continued to carry salty waters (35.1 g/kg with a standard deviation of 0.2 g/kg) into the Solomon Sea.

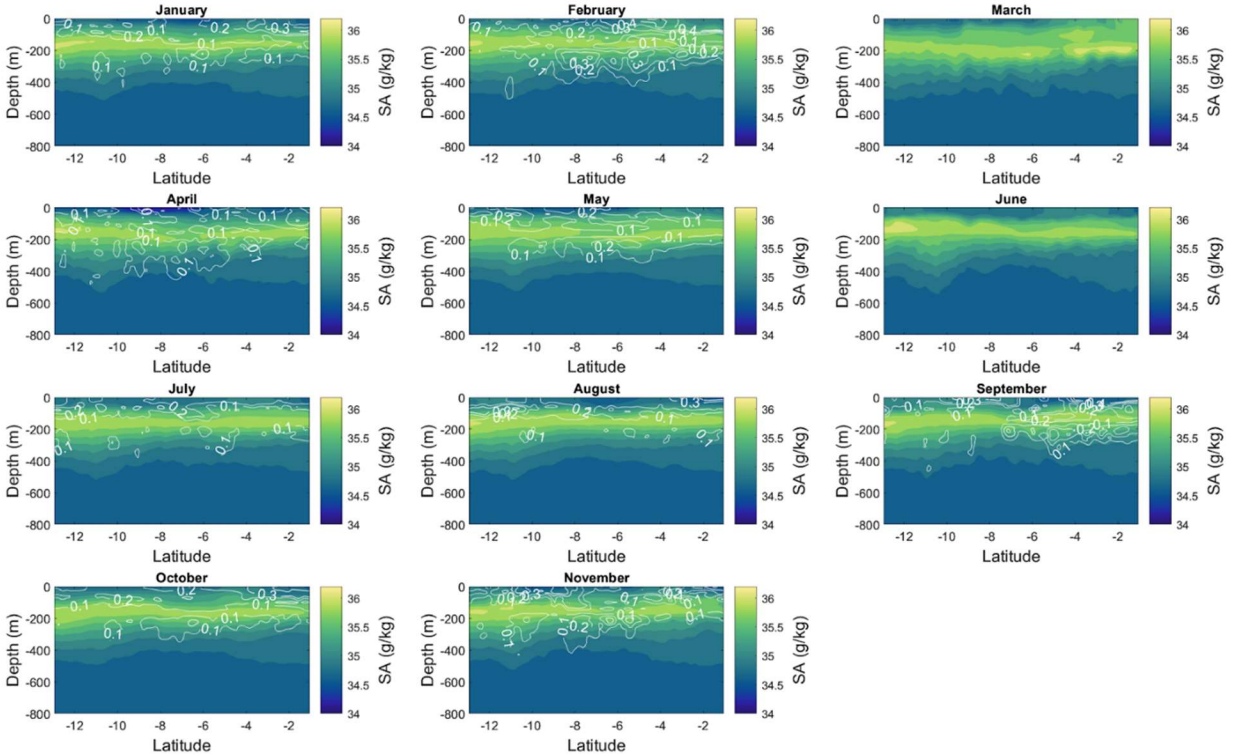

Figure 14. Argo+HR-XBT+Altimetry derived monthly absolute salinity with standard deviations along the nominal PX05 route from 13°S-1°S (encompassing the Solomon Sea to the equator).

In austral spring (August-October), fresh surface waters (34.7 g/kg with a standard deviation of 0.2 g/kg) pooled over the northern Solomon Sea and equatorward (8°S-5°S in August, 6°S-1°S in September, and approximately 3°S-1°S in October). Salinity maximums (36.0 g/kg

with a standard deviation of 0.1 g/kg) returned to the thermocline level south of the Louisiade Archipelago (12°S) in August and September, as well as a more clearly defined NGCU (identified by the dips in the isohalines) than was detected by the Argo+HR-XBT+Altimetry salinity measurements in October.

In their comparison of March 2014 and July-August 2012 (opposing trade wind seasons), Germineaud et al. (2016) found waters carried out of the Solomon Sea by the NGCU and SGU were saltier in March than in July. Germineaud et al. (2016) also found that the salty waters of SLW depths were confined east of the Solomon Islands in March, and both the NVJ and GPC carried salty waters into the Solomon Sea. In July of 2012, Germineaud et al. (2016) observed the SLW (24 kg/m^3 - 26 kg/m^3) spread from the eastern Pacific to the Solomon Strait and characterized the NGCU as a salty current gaining freshness along its equatorward pathway. Germineaud et al. (2016) traced the AAIW into the Solomon Sea in August and suggested the SLW experiences property modifications as it is carried northward by the NGCU.

4.3 Monthly Mean Geostrophic Velocity

Argo+HR-XBT+Altimetry data portrayed the NVJ as slowest (≤ 0.1 m/s) from late austral summer through austral fall (January-April; Figure 15). The NVJ was fastest (≤ 0.2 m/s) from mid-austral spring into austral summer (September-December). The NVJ widened between July and January.

Argo+HR-XBT+Altimetry data suggested that the GPC has two maximum velocity cores. The southern core (~12°S centered near 425 m) and northern core (~11.15°S centered near 300 m) both flowed at speeds under 0.2 m/s, though the southern core was slower than the northern core. Both cores extended to the surface when the GPC strengthened in austral fall and austral winter (February-June). In May, the northern flow more than doubled in speed at the surface (≤ 0.3 m/s).

Argo+HR-XBT+Altimetry data found two cores of the NGCU/NGCC system, and although the southern core was often stronger, the two frequently seemed to strengthen or weaken together. The southern branch (~10.3°S) often had a maximum velocity core centered near 230 m that rose in the water column when speeds increased. The northern core (~9.15°S) was shallower (centered near 150 m) than the southern core and more often reached the surface during times of strengthening. Argo+HR-XBT+Altimetry core depths were far shallower than the central core depth of 500 m reported by Germineaud et al. (2016) during July and August 2012. Both NGCU/NGCC cores were weaker between January to June and stronger between July and December. The southern core was weakest (~0.2 m/s) in February and May and the northern core was weakest (~0.15 m/s) February-April. The southern core was strongest in September and October (~0.3 m/s) and the northern core was strongest (~0.3 m/s) in August and September. Argo+HR-XBT+Altimetry observations partially met Melet et al.'s (2010) expectations of western boundary currents weakening in austral fall (February-April). Germineaud et al. (2016) reasoned western boundary currents strengthen in austral winter (May-July) due to a combination of local wind influence and Rossby waves, which partially aligned with Argo+HR-XBT+Altimetry observations.

The central Solomon Sea's (~8°S) eastward surface velocities neared 0.45 m/s eight months of the year: March, April, May, August, September, October, November, and December. These eastward velocities slowed to 0.3 m/s in January and June, and to 0.25 m/s in February.

The flow reversals nestled between the central Solomon Sea and the Solomon Sea inflow often flowed at similar speeds (both have a "general" time-mean speed $\leq 0.17 \pm 0.6$ m/s). In June however, the eastward flow (6°S) overtook the westward flow (7°S) and the two reached speeds up to 0.25 m/s or 0.05 m/s, respectively. A connection between the eastward surface flow (6°S)

and the NBCU was also formed in June, meaning eastward velocities continued between the surface flow at 6°S and the NBCU. The eastward velocities between the surface flow (6°S) and the NBCU persisted for half of the year (June-November) and separated the underlying westward velocities from the Solomon Sea inflow. In contrast, westward velocities extended from the Solomon Sea inflow to deeper depths between December and May. The Solomon Sea inflow was weakest in March (≤ 0.22 m/s) and strongest July-September (≤ 0.4 m/s, ≤ 0.45 m/s, and 0.4 m/s respectively).

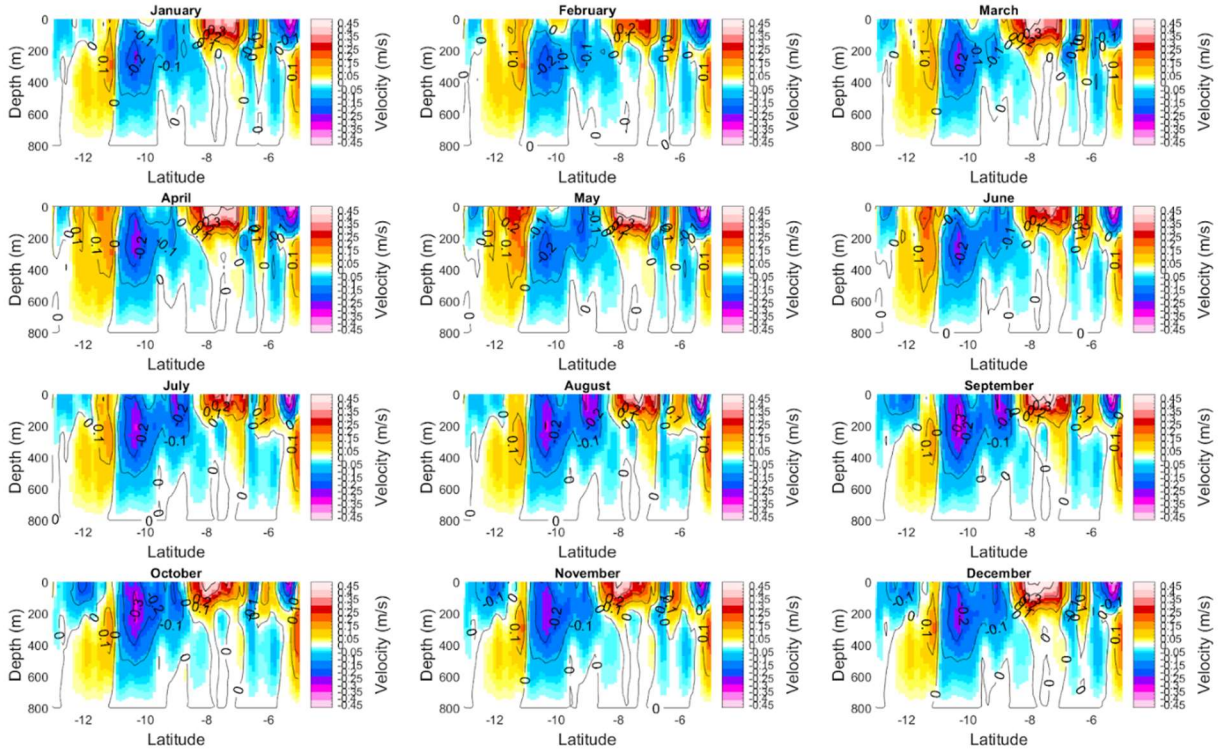

Figure 15. Argo+HR-XBT+Altimetry derived monthly geostrophic velocity along the nominal PX05 route from 13°S-5°S (encompassing the Solomon Sea).

Germineaud et al. (2016) suggested the NBCU is weak and less confined to New Britain in austral summer (November-January), however Argo+HR-XBT+Altimetry data indicated that the NBCU was weakest (~0.01 m/s) in April and May. The NBCU most often flowed at speeds ≤ 0.2 m/s, however in October the NBCU picked up to 0.22 m/s. Melet et al. (2010) anticipated the

NBCU to be at its maximum in austral spring (August-October). It is likely that the cut off at 5°S impacted this study's ability to fully examine the seasonal variability of the NBCU.

The model study of Melet et al. (2010) indicated western boundary currents within the Solomon Sea weaken in austral fall (February-April). Melet et al. (2010) reasoned weakening is caused in part by a remotely forced Rossby wave due to the western subtropical gyre spinning down (leading to clockwise anomalous circulation, i.e., the strengthening of the NQC and weakening of the NVJ). Melet et al. (2010) further reasoned these phenomena cause waters in the central and southern Solomon Sea (7°S-11°S) to exit through the Indispensable Strait and led to the intensification of the SEC during austral fall. The model study of Melet et al. (2010) also suggested the NVJ is stronger than usual during austral summer (November-January) due to the western subtropical gyre spinning up and inducing anticyclonic eddies across the subtropical gyre. In consequence, the NGCU and NBCU were anticipated to strengthen in austral summer. Neither of these expectations perfectly align with the strengthening and weakening of the NVJ and NGCU provided by the Argo+HR-XBT+Altimetry dataset.

5. Summary

5.1 Objectives

Improving our understanding of pathways within the South Pacific LLWBC system better equips scientists to understand property transports (e.g., heat, salt, mass) between the South Pacific subtropical gyre and the Equatorial Pacific. In supplying the EUC, ITF, and Western Pacific Warm Pool, the South Pacific LLWBCs impact global thermohaline circulation, atmospheric convection, and global climate modulations like ENSO. The purpose of this study was to investigate spatial (i.e., depth, width) and temporal (i.e., monthly, seasonal) variability of the circulation patterns within the Solomon Sea, which had long evaded scientific exploration due to complex bathymetry.

Using long-term temperature observations from HR-XBTs (2009-2019), sea surface height from satellite altimetry (2004-2019), and temperature-salinity profiles from the Argo network (2004-2019), this study describes characteristics of the upper 800 m of the South Pacific LLWBCs and their pathways, while also providing an enhanced view of the region's seasonal variability through observations based on a near 16-year period.

Argo climatology was used to interpolate dynamic height (0/1975 m) across the Solomon Sea and in creating the combined Argo+HR-XBT dataset. Following Chandler et al. (2021) and Zilberman et al. (2018), temperature and salinity were projected onto the nominal PX05 transect using horizontal temperature and salinity gradients from Argo climatology. Mean calculations of conservative temperature, absolute salinity, dynamic height, geostrophic velocity, and depth-integrated geostrophic velocity were made along the nominal PX05 transect. Standard deviations were calculated for conservative temperature, absolute salinity, potential density, and geostrophic velocity examinations.

A linear regression between the 13-day averaged SLA and steric height's temporal anomaly was calculated using Argo data along the nominal PX05 HR-XBT transect. This produced monthly geostrophic velocity with use of the thermal wind equations across the nominal PX05 transect relative to a level of no motion (800 m or shallower bathymetry levels; Chandler et al. 2021). The Argo+HR-XBT+Altimetry dataset enabled monthly and seasonal inspections of conservative temperature, absolute salinity, and geostrophic velocity (including standard deviations for conservative temperature and absolute salinity). Future studies may wish to extend the Argo+HR-XBT+Altimetry measurements to 1975 m following Zilberman et al. (2018) and Chandler et al. (2021), as well as consider a shallower reference level (e.g., an Argo profile depth

selection of 1400 m instead of 1975 m) to maximize the Argo sampling in the shallow regions of the Solomon Sea.

5.2 Water Properties

The near 16-year mean temperature observations from the Argo+HR-XBT dataset depicted the mixed layer deepening towards the equator in agreement with the model study of Melet et al. (2010). The seasonal Argo+HR-XBT+Altimetry observations of conservative temperature demonstrated little variability apart from a deepening of the mixed layer from March to May. The low variability in temperature reflects the low variability of solar radiation received at the equator, and the deepening mixed layer may result from wind or evaporative processes that affect surface density and vertical convection. The isothermal dips that indicated the presence of the NGCU were not well-defined in March or July, but otherwise detectable as the NGCU carried warmer water equatorward at 240 m or below in the remaining observed months.

Argo+HR-XBT mean salinity observations reinforced the presence of SPTW (salinity maximum) at thermocline levels and confirmed the Solomon Strait as a passage for relatively high-salinity surface waters to enter the Solomon Sea. We speculate the Solomon Strait inflow sinks underneath the freshwater layers within the Solomon Sea and mixes with the SPTW near 7°S-5°S. SPTW was previously noted in thermocline levels by Anutaliya et al. (2019), Germineaud et al. (2016) and Ganachaud et al. (2014; considering the density of UTW corresponds to the density of SPTW). Argo+HR-XBT mean salinity observations provided unforeseen detail on a shallow, freshwater pool in the central Solomon Sea, which monthly Argo+HR-XBT+Altimetry observations found to extend further northward in austral spring (August-October). Finally, the isohaline dips used to identify the NGCU obscured in February, March, and October.

Mean Argo+HR-XBT density affirmed the presence of SPTW, SPSTW (also called STMW), SLW, SAMW, and AAIW within the Solomon Sea (13°S-1°S) as reported by others (Anutaliya et al. 2019; Germineaud et al. 2016). Argo+HR-XBT measurements detected SPTW in an upper thermocline level (density of 24.5 kg/m^3), and SPSTW in the lower thermocline levels (density of 25.5-26 kg/m^3; Germineaud et al. 2016 and Anutaliya et al. 2019). SLW (24.5-26 kg/m^3) is comprised of SPTW and SPSTW. Argo+HR-XBT measurements found SLW in the thermocline above SAMW (26.5-27 kg/m^3, Germineaud et al. 2016). Argo+HR-XBT densities support AAIW (26.9-27.4 kg/m^3) residing in the lower NGCU and Solomon Strait, however investigations of water mass characteristics such as oxygen, nitrogen, and silica may create a clearer picture (Germineaud et al. 2016).

Argo+HR-XBT observations demonstrated waters below the thermocline were saltier equatorward and waters above the thermocline were warmer equatorward. A model of tidal mixing by Melet et al. (2011), a numerical simulation by Grenier et al. (2011), and global simulations of internal wave activity by Simmons et al. (2004) suggested the Solomon Sea and downstream are regions of strong mixing (Ganachaud et al., 2014). Alberty et al. (2017) concluded from observations that mixing varied vertically, horizontally, and seasonally within the Solomon Sea. For instance, Alberty et al. (2017) found that mixing was stronger at shallower depths than lower depths, and stronger mixing occurred above underwater ridges and seamounts while weaker mixing occurred where the seafloor was smooth and flat (in result of tides and internal waves). Finally, Alberty et al. (2017) anticipated that seasonal mixing follows the strength of monsoonal winds. The mixing processes of shallower depths remains poorly understood. Further research may provide insight on the relationship of the monsoon seasons and eddy activity to water property modifications in the Solomon Sea and their anticipated impact on the equatorial region.

5.3 Pathways

Argo+HR-XBT mean observations described a shallow NVJ core (0.12 m/s with a standard deviation of 0.3 m/s in the upper 60 m) encountering the GPC over the near-16-year period. The NVJ was slowest (≤ 0.1 m/s) in late austral summer and austral fall (January-April), and fastest (≤ 0.2 m/s) mid-austral spring into mid-austral summer (September-December). The NVJ narrowed February-June and had the widest horizontal extent July through January.

The high-velocity GPC and NGCU cores over the near 16-year time-mean (Figure 8) supports the consensus that the GPC feeds into the NGCU (Ganachaud et al. 2014; Germineaud et al. 2016; Alberty et al. 2019). Ganachaud et al. (2014) described the GPC core as centered near 400 m and Germineaud et al. (2016) described the NGCU as centered near 500 m depth, while the model study of Melet et al. (2010) placed the NGCU core as flowing at speeds of 20 cm/s between 100 m and 300 m depth. Argo+HR-XBT analysis placed the GPC and NGCU cores near 230 m depth and provided geostrophic velocities of 0.19 m/s (with a standard deviation of 0.2 m/s) and 0.26 m/s (with a standard deviation of 0.3 m/s), respectively.

The model study of Melet et al. (2010) indicated the Solomon Sea's western boundary currents strengthen in austral summer (November-January) and weaken in austral fall (February-April), partially reflecting Argo+HR-XBT+Altimetry observations. The GPC exhibited two core placements in monthly Argo+HR-XBT+Altimetry measurements (each between 0.1-0.2 m/s from July to March with the northern core traveling faster). When the GPC strengthened (April-June) the core placements rose in the water column (concurrent with the narrowing of the NVJ) and the distinction between the two cores blurred (e.g., July-January had two well-defined regions of greater velocity whereas April-June was almost completely defined by greater velocity).

The variability of the GPC's core placements may impact downstream western boundary currents in two ways: (1) a modification of the properties carried into the Solomon Sea as the GPC alternates in coverage and strength with the NVJ at the southern entrance; and (2) its role as a source water for the NGCU. Germineaud et al. (2016) described the NVJ to carry high salinity and high oxygen waters into the Solomon Sea, while the GPC carries fresher and more highly oxygenated water into the Solomon Sea. One can reason that water properties downstream will reflect whichever current is dominating the southern entrance of the Solomon Sea, yet more research is required to fully understand the impact of the two current's unique water properties (e.g. their impact on biological production). The stronger months of the GPC (February-June) largely coincided with the weaker months of the NGCU/NGCC system (January-June) and vice versa. The GPC and NGCU cores appear better aligned in the water column in the months that the two are weaker (both the GPC and NGCU/NGCC cores rise in the water column when strengthened). Further research is required to fully understand the relationship between the GPC and the NGCU/NGCC system, as well as what contributes to the strengthened velocities in the currents. The strengthening of the westward NVJ and westward NGCU/NGCC near the same months suggests South Pacific LLWBC strengthening is linked to larger forcings.

Time-mean geostrophic velocities from Argo+HR-XBT measurements exhibited powerful surface currents (0.42 m/s with a standard deviation of 0.6 m/s) within the central Solomon Sea. The persistence of the fast eastward velocities over the near 16-year observational period suggests them to be a permanent feature.

The Solomon Strait is the most notable source of incoming surface waters to the northern Solomon Sea (Anutaliya et al. 2019; Ganachaud et al. 2014; Melet et al. 2010). Anutaliya et al. (2019) wrote that the Solomon Strait inflow is primarily confined to the northern and eastern basin,

and suggested the Solomon Strait inflow of the eastern basin contributes to a poleward surface flow exiting the southern Solomon Sea. It is possible that the strong eastward flows of the central Solomon Sea also connect the Solomon Strait inflow to poleward surface waters exiting the southeastern Solomon Sea. Further investigation of the source and destination of the strong, shallow, and persistent flow in the central Solomon Sea could uncover if the flow does indeed connect northern and southern surface waters.

The central Solomon Sea's eastward surface velocities (0.42 m/s with a standard deviation of 0.6 m/s) and the Solomon Sea inflow (0.38 m/s with a standard deviation of 0.6 m/s) demonstrated little monthly fluctuation in Argo+HR-XBT-Altimetry observations. More often the eastward surface velocities of the central Solomon Sea strengthened to 0.45 m/s, but they weakened to 0.3 m/s in January and June, and to 0.25 m/s in February. The Solomon Sea inflow was weakest in March (~0.22 m/s) and strongest in July, August, and September (0.4-0.45 m/s).

Beneath the Solomon Sea inflow lies the outflowing NBCU (mean velocity of 0.24 m/s and a standard deviation of 0.3 m/s). The maximum velocities of the NBCU by Argo+HR-XBT data are a fraction of the speed (0.6 m/s) described by the model analysis of Melet et al. (2010). Alberty et al. (2019) and Melet et al. (2010) center the NBCU core equal to or above 250 m depth, however the Argo+HR-XBT dataset found a NBCU core lower in the water column (260-450 m depth). Argo+HR-XBT+Altimetry suggested the NBCU is weakest from April-May (~0.1 m/s) and strongest in October (0.22 m/s), which is unlike Germineaud et al. (2016) who suggested that the NBCU is weak and less confined to New Britain in austral summer (November-January). The maximum encountered in October is in-line with Melet et al. (2010) who anticipated that the NBCU experiences its maximum in austral spring (August-October). Argo+HR-XBT+Altimetry measurements also illustrated eastward velocities connecting the NBCU to one of the many flow

reversals found between the northern Solomon Sea and the equator six months of the year (June-November).

The NICU may require great attention since existing descriptions only somewhat align with Argo+HR-XBT observations. Melet et al. (2010) and Butt and Lindstrom (1994) centered the NICU near 230 m with speeds near 0.6 m/s. Argo+HR-XBT data portrayed three flows partially fitting the provided NICU description: a 0.31 m/s (with a standard deviation of 0.5 m/s) core centered near 200 m at 3.45°S, a 0.55 m/s (with a standard deviation of 0.6 m/s) flow residing in the upper 180 m at 3°S, and a 0.41 m/s (with a standard deviation of 0.6 m/s) flow in the upper 170 m at 2.15°S. Continued research is required to properly describe the NICU, and therefore improve our understanding of the most direct pathway thermocline waters within the South Pacific LLWBC system take to the equator.

This study provides high-resolution observations of the speeds and depths of flow reversals nearing the equator (Figure 8). Among the many flow reversals were two eastward subsurface flows. Argo+HR-XBT observations centered the first core at 340 m (0.16 m/s with a standard deviation of 0.3 m/s at 2.35°S) and the second near 210 m (0.39 m/s with a standard deviation of 0.6 m/s at 1.25°S). Butt and Lindstrom (1994) detected an eastward flow at 240 m depth near 2°S, yet documentation on the many surface flow reversals and subsurface flows have been scarce. Further research is required to discern the source and destination of the surface and subsurface flows found near the equator.

This study considered depth-integrated geostrophic velocity in the upper 0-800 m, 0-150 m, and lower 160-800 m. The 150-m cut off was selected based on Figure 8, with the intention of keeping the surface and subsurface cores primarily intact. Most often the upper (0-150 m) and lower (160-800 m) sections flowed in similar directions with the lower section hosting the greater

depth-integrated velocity. The highest depth-integrated velocities were those of the GPC (0.85 m^2/s at 11.15°S), the NGCU (southern core, 122.72 m^2/s at 10.35°S), the NBCU (107.34 m^2/s at 4.95°S), the NICU (135.60 m^2/s at 2.85°S), and an unnamed eastward flow (111.78°S m^2/s at 1.25°S). The eastward flows within the central Solomon Sea have larger depth-integrated velocities in the upper 150 m than in their 160-800 m counterparts (42.94 m^2/s versus 37.93 m^2/s respectively) due to wind-driven contributions. All depth-integrated velocities emphasized the two-peak features of the GPC and NGCU/NGCC system. One can reason the islands of the Louisiade Archipelago split the GPC into two streams. It is unclear why the NGCU and NGCC are broken up into two streams.

5.4 Next Steps

While this study improves our understanding of the pathways and characteristics of the South Pacific LLWBCs by providing long-term and seasonal observations along the nominal PX05 route, there are several uncertainties remaining. For instance, this study did not address the southeastern Solomon Sea, which is believed to host many mesoscale eddies, poleward outflow, and alternating flow directions within the Indispensable Strait (Anutaliya et al. 2019; Ganachaud et al. 2014; Melet et al. 2010). Furthermore, the NICU and eastward flow in the central Solomon Sea need clarification, and the SICU remains only a modeled prediction unconfirmed by observations despite its potential contributions to the South Pacific LLWBC system.

The Argo+HR-XBT and Argo+HR-XBT+Altimetry datasets indicate that high-resolution calculations of long-term and seasonal transport within the South Pacific LLWBC system are attainable. The South Pacific LLWBC system supplies roughly two thirds of the EUC's transport to the Central Pacific, and the pathways which the transports take (i.e., Vitiaz Strait, St. George's Channel, Solomon Strait) affect both transit times and mixing rates (Alberty et al. 2019). Mixing

rates and transit times influence the upper/lower and southern/northern hemisphere structure of the EUC (Alberty et al. 2019). South Pacific LLWBC transport also influences ITF, which impacts the Indian Ocean and global thermohaline circulation (Lukas et al. 1996).

To better understand the South Pacific LLWBCs' role in thermohaline circulation, one may investigate the water masses of the Solomon Sea. It is expected that water masses in the South Pacific LLWBCs experience significant modifications in their journey equatorward (Germineaud et al. 2016). Both diapycnal and isopycnal mixing seem especially active within the Solomon Sea, (Ganachaud et al. 2014; Melet et al. 2010). Continued tracking of chemical properties (e.g., iron, oxygen, nitrogen) would assist in mapping mixing water masses and aid in predicting primary productivity as far as the Central Pacific (Alberty et al. 2019).

Assessing the South Pacific LLWBCs on interannual and decadal timescales will be more meaningful in understanding the South Pacific LLWBCs' relationship with ENSO. Anutaliya et al. (2019) concludes that ENSO can highly impact equatorward flow and even stifle the seasonal cycles of prominent currents in the Solomon Sea (e.g., the NGCU/NGCC are suppressed during El Niño). Since ENSO can significantly influence thermocline transport variability in the Solomon Sea, it has major implications on water mass transport between the South Pacific and Equatorial Pacific (Alberty et al. 2019).

5.5 Acknowledgements

High Resolution Expendable Bathythermograph (HR-XBT) data is made available by the Scripps Institution of Oceanography High Resolution XBT/XCTD Program (http://www-hrx.ucsd.edu/). Argo data was collected and made freely available by the International Argo Program and the national programs that contribute to it (http://www.argo.ucsd.edu, http://argo.jcommops.org). The Argo Program is part of the Global Ocean Observing

System. High-resolution Argo climatology is available at http://sio-argo.ucsd.edu/RG_Climatology.html. Satellite altimetry is made available by Copernicus Marine Service (https://marine.copernicus.eu/).

The thesis author was the primary investigator and author of this paper. While the discovery of the shallow, fast, and persistent flow in the central Solomon Sea appears new to oceanographic literature, it may be familiar to Indigenous peoples. Therefore if future investigations confirm this flow as part of a surface current, they are implored to consider the knowledge of Indigenous peoples as much as oceanographic literature.

REFERENCES

Alberty, M. S., Sprintall, J., MacKinnon, J., Ganachaud, A., Cravatte, S., Eldin, G., Germineaud, C., & Melet, A., (2017), Spatial patterns of mixing in the Solomon Sea, *Journal of Geophysical Research: Oceans*, 122, 4021–4039, doi:10.1002/ 2016JC012666.

Alberty, M., Sprintall, J., MacKinnon, J., Germineaud, C., Cravatte, S., & Ganachaud, A. (2019). Moored observations of transport in the Solomon Sea. *Journal of Geophysical Research: Oceans*, 124, 8166–8192. https://doi.org/10.1029/2019JC015143

Anutaliya, A., Send, U., Sprintall, J., McClean, J. L., Lankhorst, M., & Koelling, J. (2019). Mooring and seafloor pressure endpoint measurements at the southern entrance of the Solomon Sea: Subseasonal to interannual flow variability. *Journal of Geophysical Research: Oceans*, 124, 5085–5104. https://doi.org/10.1029/ 2019JC015157

Argo (2000). Argo float data and metadata from Global Data Assembly Centre (Argo GDAC). SEANOE. http://doi.org/10.17882/42182

Butt, J., & Lindstrom, E., (1994) Currents off the east coast of New Ireland, Papua New Guinea, and their relevance to regional undercurrents in the Western Equatorial Pacific Ocean. *Journal of Geophysical Research*, Vol 99, NO. C6, Pg 12,503 – 12,514

Chandler, M., Zilberman, N. V., Sprintall, J., (2021) Combining Complementary Observing Systems to Produce a Basin-Scale Network For Monitoring Upper-Ocean Transport. Scripps Institution of Oceanography. https://escholarship.org/uc/item/7pg5m20c

Ganachaud, A., Cravatte, S., Melet, A., Schiller, A., Holbrook, N. J., Sloyan, B. M., Widlansky, M. J., Bowen, M., Verron, J., Wiles, P., Riggway, K., Sutton, P., Sprintall, J., Steinberg, C., Brassington, G., Cai, W., Davis, R., Gasparin, F., Gourdeau, L., Hasegawa, T., Kessler, W., Maes, C., Takahashi, K., Richards, K. J., & Send, U. (2014) The Southwest Pacific Ocean Circulation and Climate Experiment (SPICE). *Journal of Geophysical Research: Oceans.* 10.1002/2013JC009678

Germineaud C., Ganachaud A., Sprintall J., Cravette S., Eldin G., Alberty M., & Privat E. (2016). Pathways and Water Mass Properties of the Thermocline and Intermediate Waters in the Solomon Sea. *Journal of Physical Oceanography*, dx.doi.org/10.1175/JPO-D-16-0107.s1

Lukas, R., T. Yamagata, & J. McCreary, (1996). Pacific low-latitude WBCs and the Indonesian throughflow. *Journal of Geophysical Research*, Volume 101, No.C5

Melet, A., Gourdeau L., Kessler, W. S., Verron, J., & Molines, J. (2010). Thermocline Circulation in the Solomon Sea: A Modeling Study. *Journal of Physical Oceanography*, Volume 40, 1302-1319. DOI: 10.1175/2009JPO4264.1

McDougall, T.J., and Barker, P.M. (2011). Getting started with TEOS-10 and the Gibbs Seawater (GSW) Oceanographic Toolbox, 28pp., SCOR/IAPSO WG127, ISBN 978-0-646-55621-5. https://www.teos-10.org/software.htm

Roemmich, D., and B. Cornuelle (1987). Digitization and calibration of the expendable bathythermograph. Deep-Sea Research, 34, 299-307

Roemmich, D. and J. Gilson (2009): The 2004-2008 mean and annual cycle of temperature, salinity, and steric height in the global ocean from the Argo Program. *Progress in Oceanography*, 82**,** 81-100

Smith, W. H. F., & Sandwell, D. T. (1997). Global Sea Floor Topography from Satellite Altimetry and Ship Depth Soundings. Science, 277(5334), 1956–1962. https://doi.org/10.1126/science.277.5334.1956

Thyng, K. M., Greene, C. A., Hetland, R. D., Zimmerle, H. M., & DiMarco, S. F. (2016). True colors of oceanography. Oceanography, 29(3), 10.

The PLANE SAILING method as described in "CELESTIAL NAVIGATION" (1989) by Dr. P. Gormley. The Australian Antarctic Division.

Zilberman, N. V., Roemmich, D. H., Gille, S. T., & Gilson, J. (2018) Estimating the Velocity and Transport of Western Boundary Current Systems: A Case Study of the East Australian Current near Brisbane. *Journal of Atmospheric and Oceanic Technology.* DOI: 10.1175/JTECH-D-17-0153.1